Electronic Supplementary Information for Dalton Transactions

Electronic Supplementary Information

Ferrocene-based multichannel molecular chemosensors with high selectivity and sensitivity for Pb(II) and Hg(II) metal cations

María Alfonso, Alberto Tárraga, * and Pedro Molina*

Departamento de Química Orgánica. Facultad de Química. Universidad de Murcia. Campus de Espinardo, E-30100 Murcia, Spain.

E-mail: pmolina@um.es; atarraga@um.es

Table of contents

2-Ferrocenil-7,8-Diphenyl-3*H*-imidazo[4,5-*f*]quinoxalines, [6a]

^{1}H NMR (400MHz, MeOD)

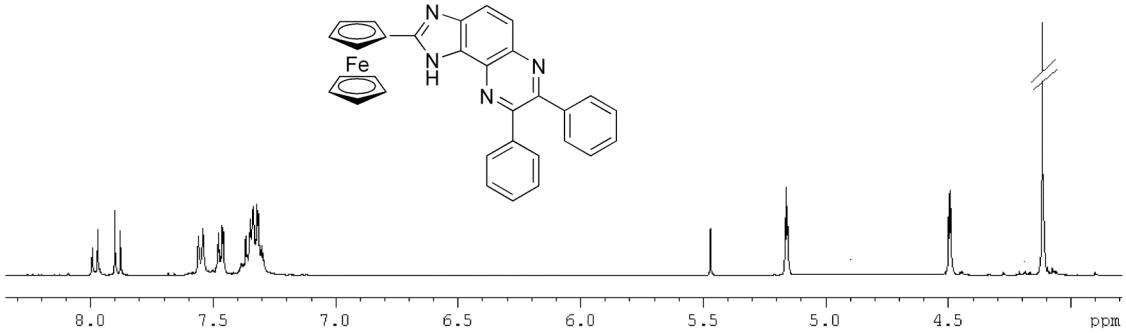

^{13}C NMR (100 MHz, $CDCl_3$):

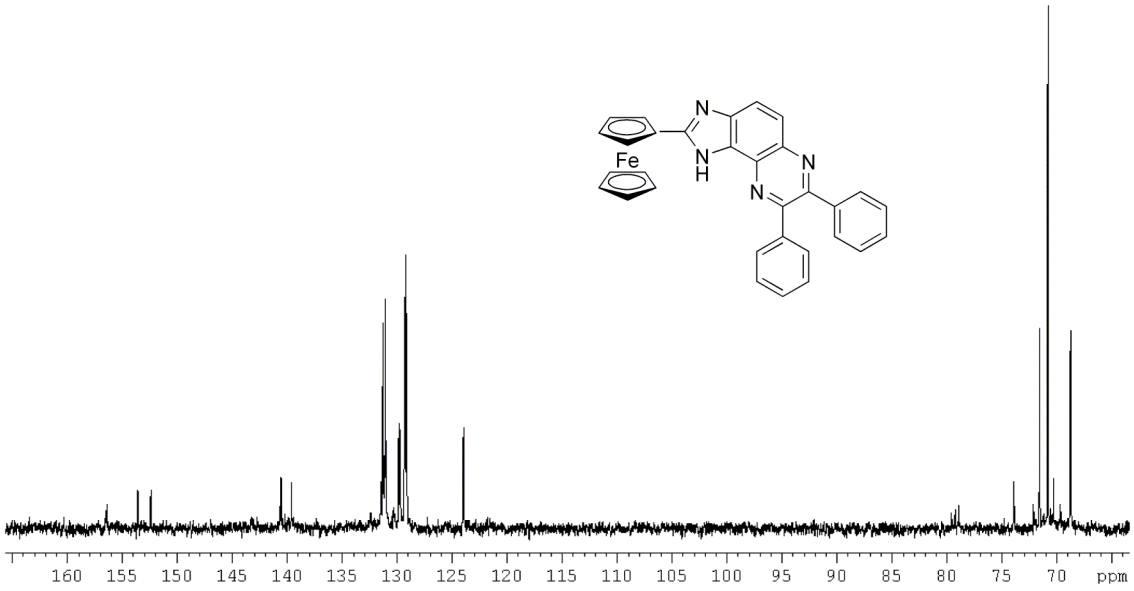

5-amino-6-nitro-2,3-di(2-pyridyl)quinoxaline, [4b]

^{1}H NMR (400MHz, $CDCl_3$)

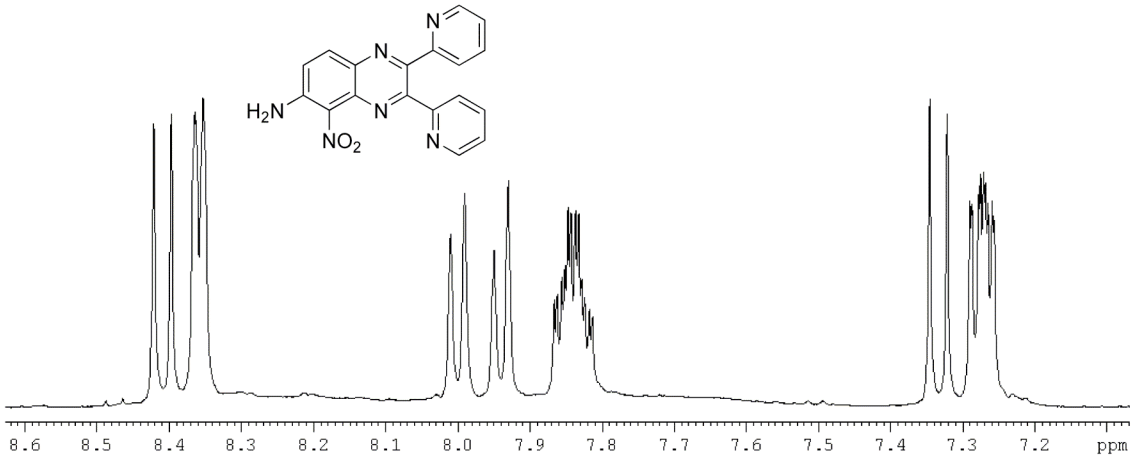

^{13}C NMR (100 MHz, $CDCl_3$):

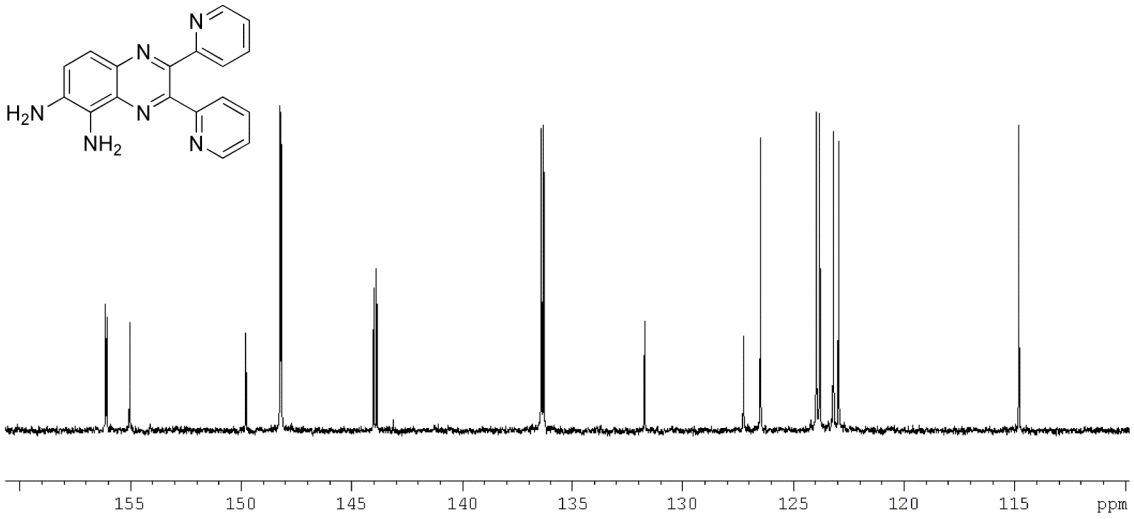

5,6-diamino-2,3-di(2-pyridyl)quinoxaline, [5b]

^{1}H NMR (400MHz, $CDCl_3$):

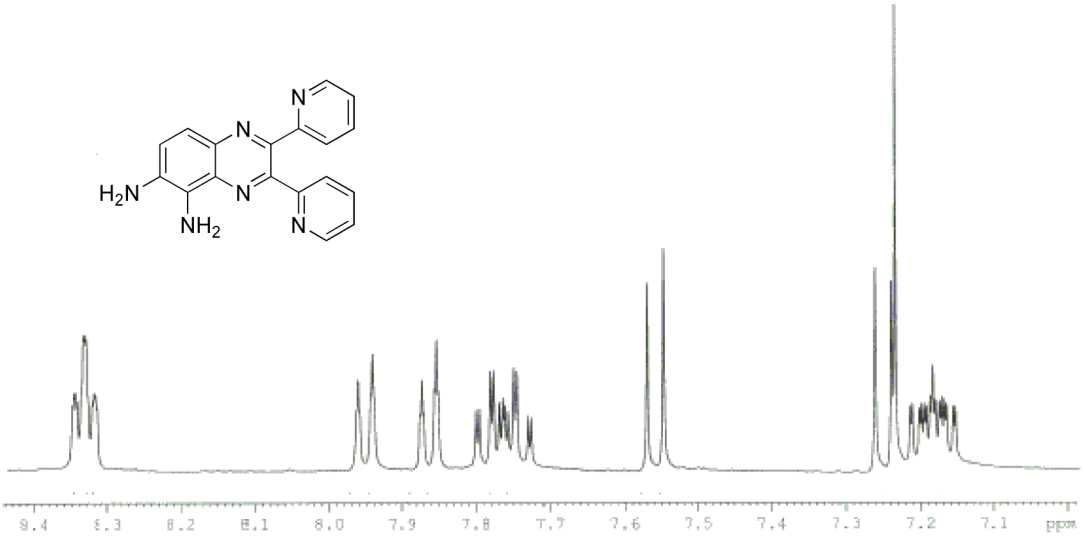

^{13}C NMR (100 MHz, $CDCl_3$):

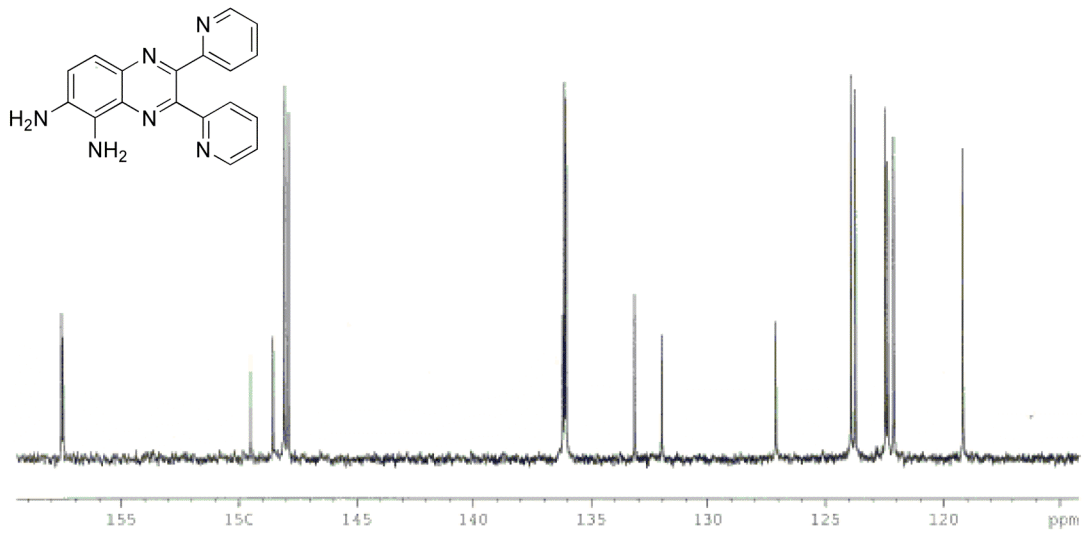

2-Ferrocenyl-7,8-Di-(2-pyridyl)-3*H*-imidazo[4,5-*f*]quinoxalines, [6b]

^{1}H NMR (400MHz, $CDCl_3$):

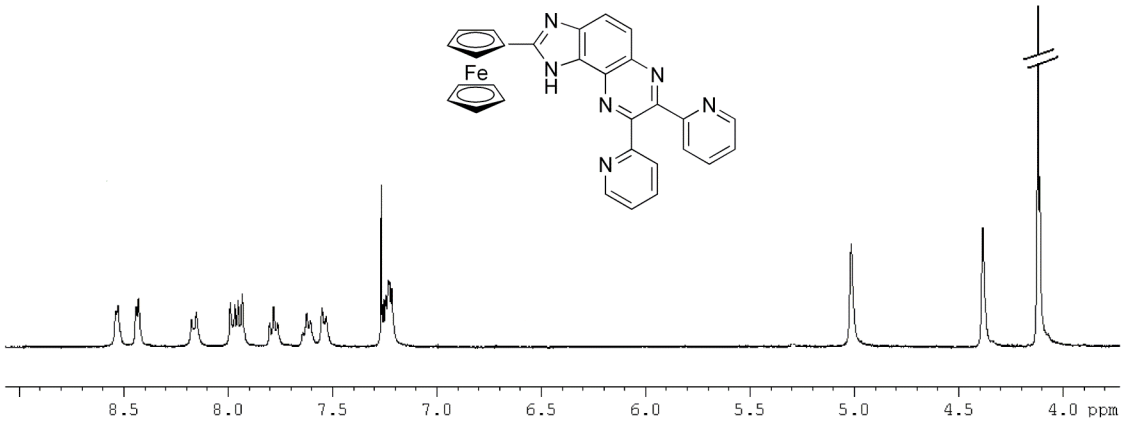

^{13}C NMR (100 MHz, $CDCl_3$):

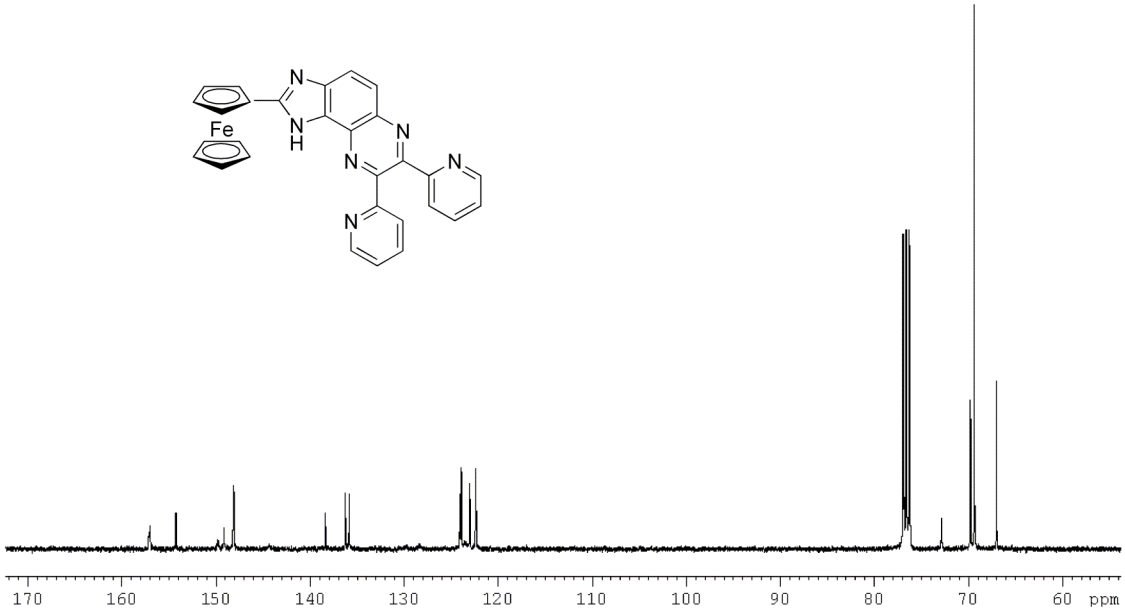

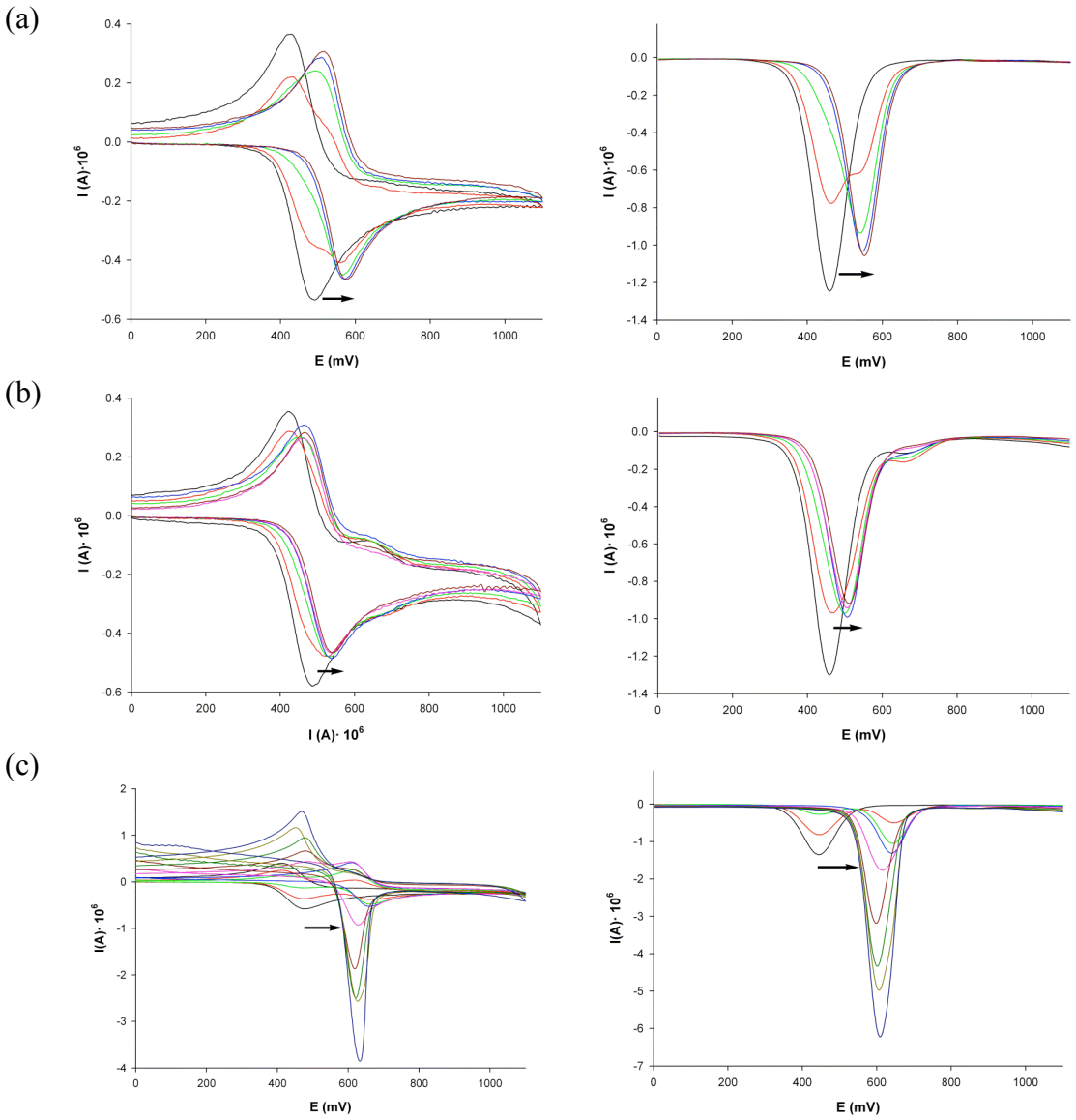

Figure SI 1. Evolution of the CV (left) and OSWV (right) of **6a** (1 mM) in CH_3CN/[(*n*-Bu)$_4$]ClO_4 scanned at 0.1 V s^{-1} in the presence of increasing amounts of: (a) Cd^{2+}; (b) Zn^{2+}; (c) Hg^{2+}.

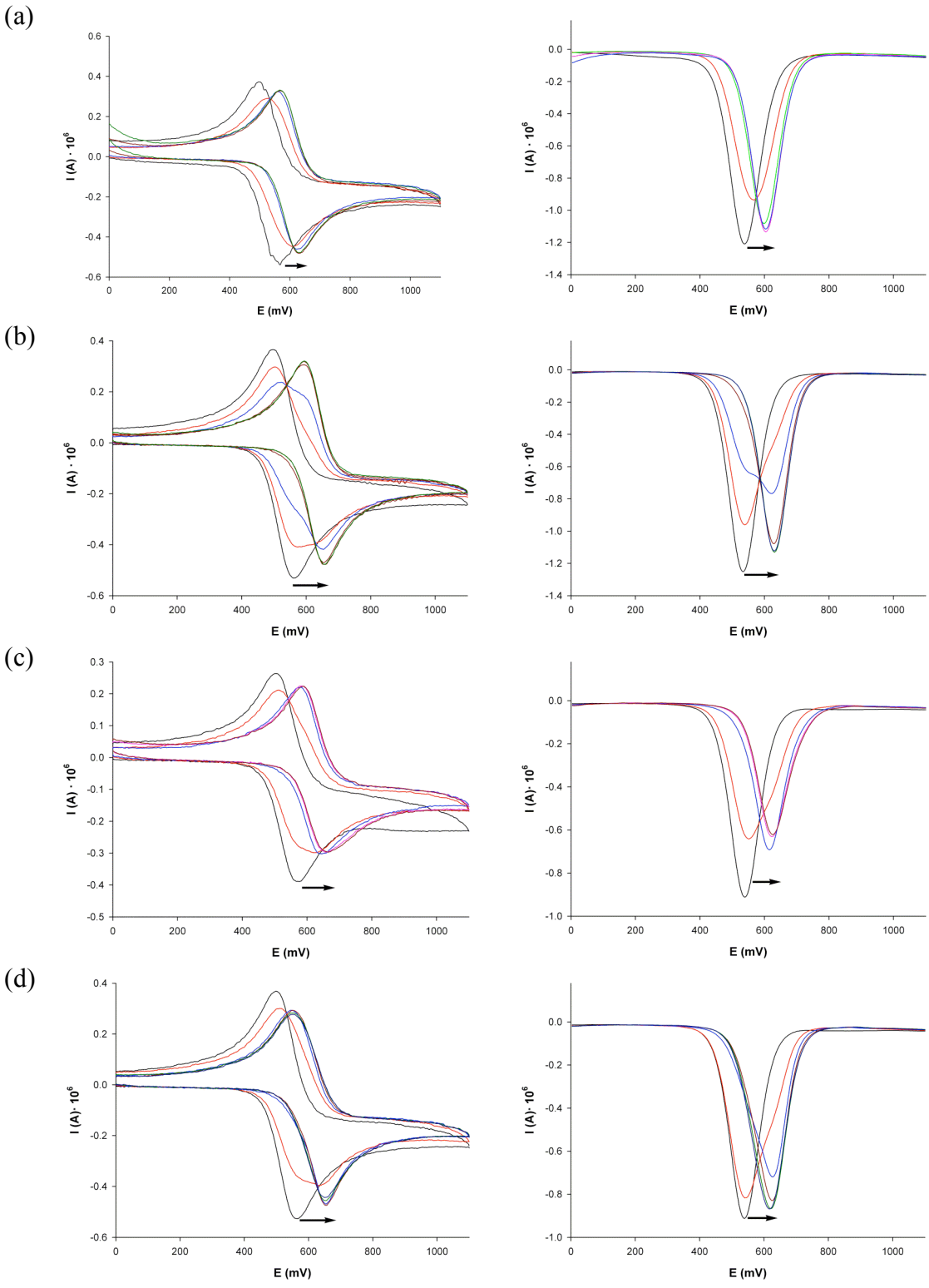

Figure SI 2. Evolution of the CV (left) and OSWV (right) of **6b** (1 mM) in CH_3CN/[(*n*-$Bu)_4$]ClO_4 scanned at 0.1 V s^{-1} in the presence of increasing amounts of: (a) Pb^{2+}; (b) Cd^{2+}; (c) Zn^{2+}; (d) Ni^{2+}.

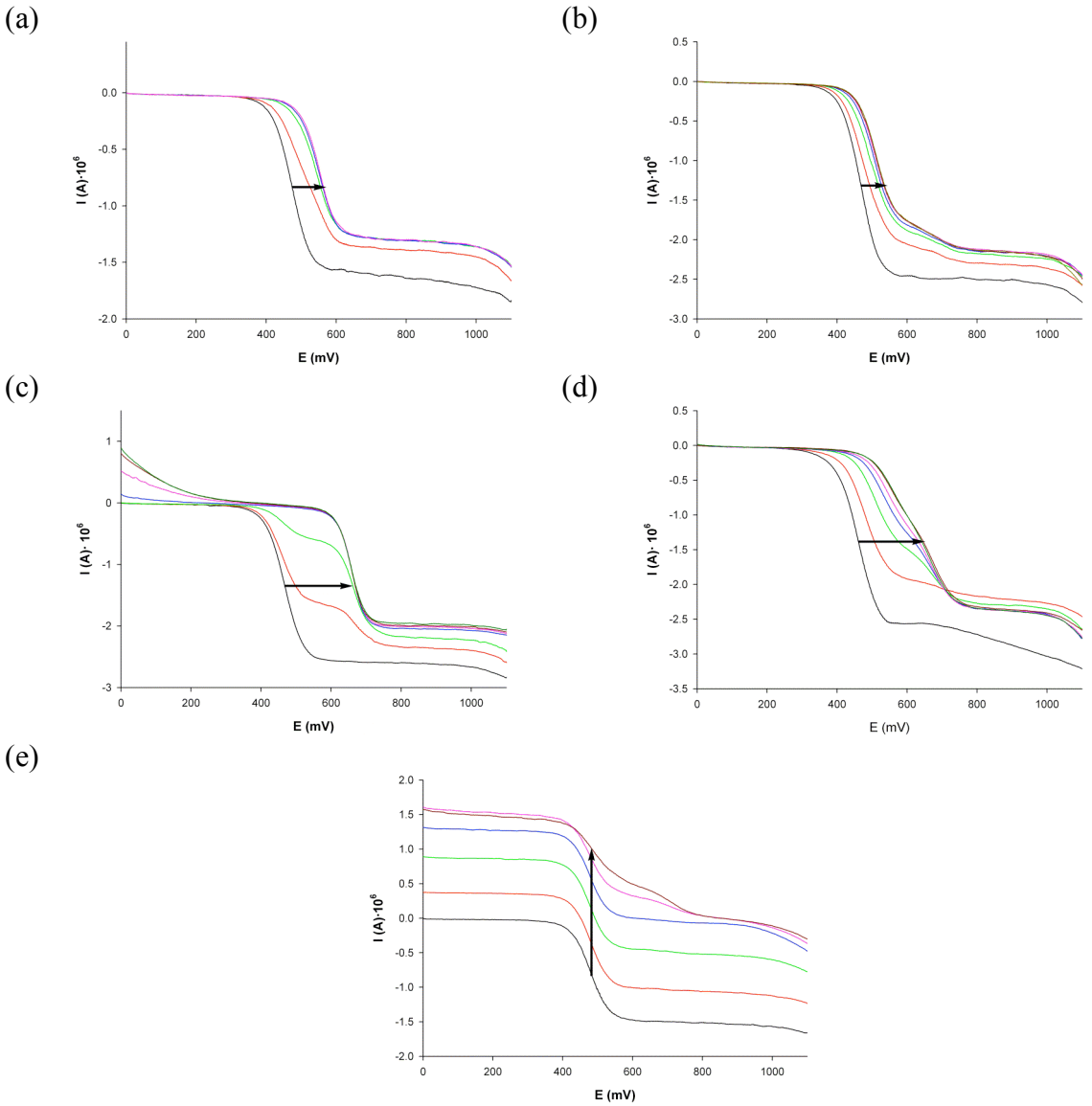

Figure SI 3. Evolution of the LSW of **6a** (1mM) in the presence of increasing amounts of (a) Cd^{2+}; (b) Cd^{2+}; (c) Hg^{2+}; (d) Pb^{2+}; (e) Cu^{2+}, obtained using a rotating disk electrode at 100 mVs^{-1} and 1000 rpm and $[(n\text{-}Bu)_4]ClO_4$ 0.1 M as supporting electrolyte.

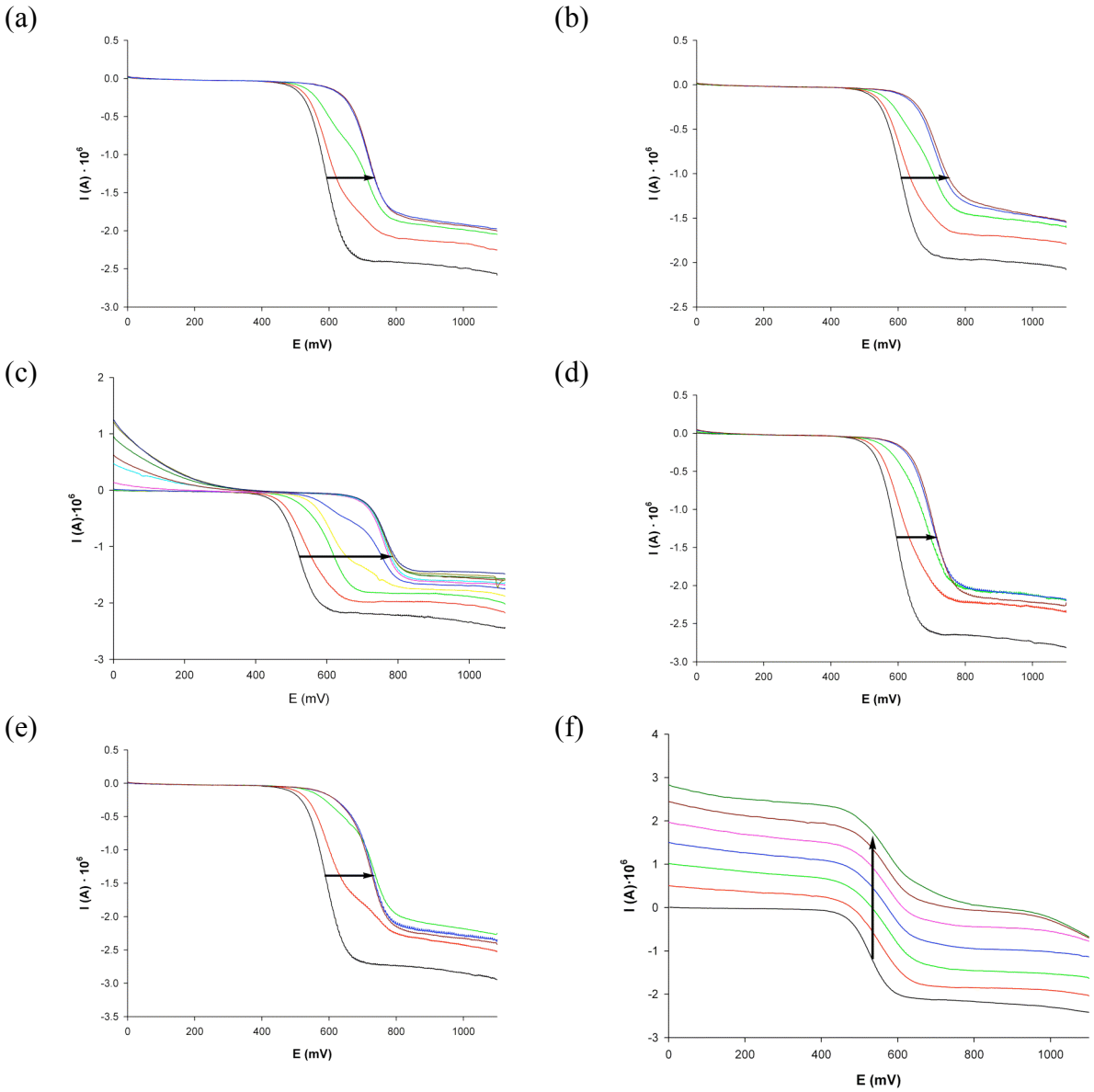

Figure SI 4. Evolution of the LSW of **6b** (1mM) in the presence of increasing amounts of (a) Cd^{2+}; (b) Zn^{2+}; (c) Hg^{2+}; (d) Pb^{2+}; (e) Ni^{2+}; (g) Cu^{2+}, obtained using a rotating disk electrode at 100 mVs^{-1} and 1000 rpm and $[(n\text{-}Bu)_4]ClO_4$ 0.1 M as supporting electrolyte.

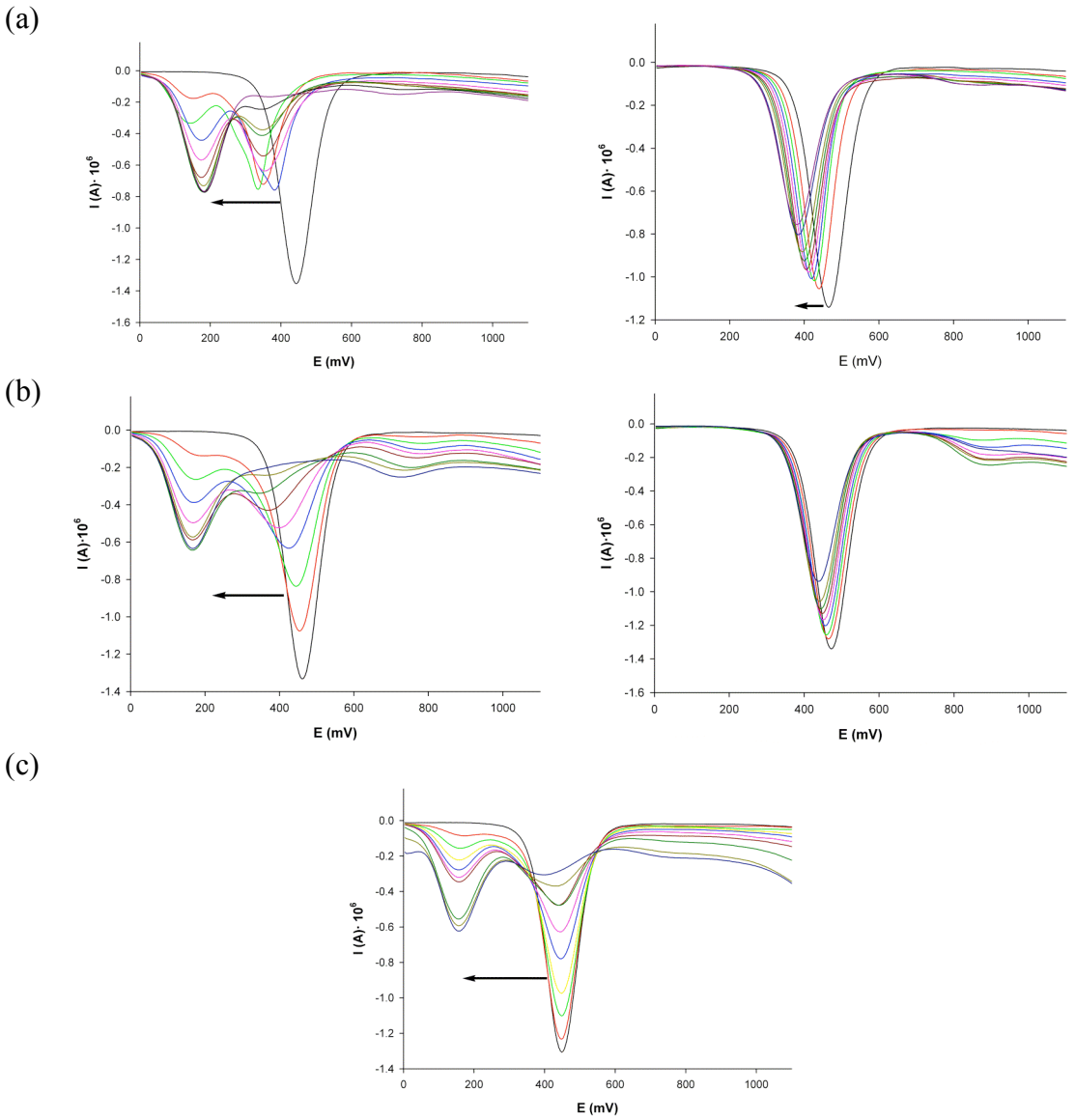

Figure SI 5. (a) Evolution of the OSWV of **6a** (1 mM) in $CH_3CN/[(n\text{-}Bu)_4]ClO_4$ scanned at 0.1 V s^{-1} in the presence of increasing amounts of (a) $HP_2O_7^{3-}$ (left) until 2 equiv and in the presence of 2 equiv of $HP_2O_7^{-3}$ and 20 equiv of acetic acid in CH_3CN (right); (b) F^- (left) until 2 equiv and in the presence of 2 equiv of F^- and 20 equiv of acetic acid in CH_3CN (right). (c) Evolution of the OSWV of **6a** (1 mM) in $CH_3CN/[(n\text{-}Bu)_4]ClO_4$ scanned at 0.1 V s^{-1} in the presence of increasing amounts of OH^- until 2 equiv.

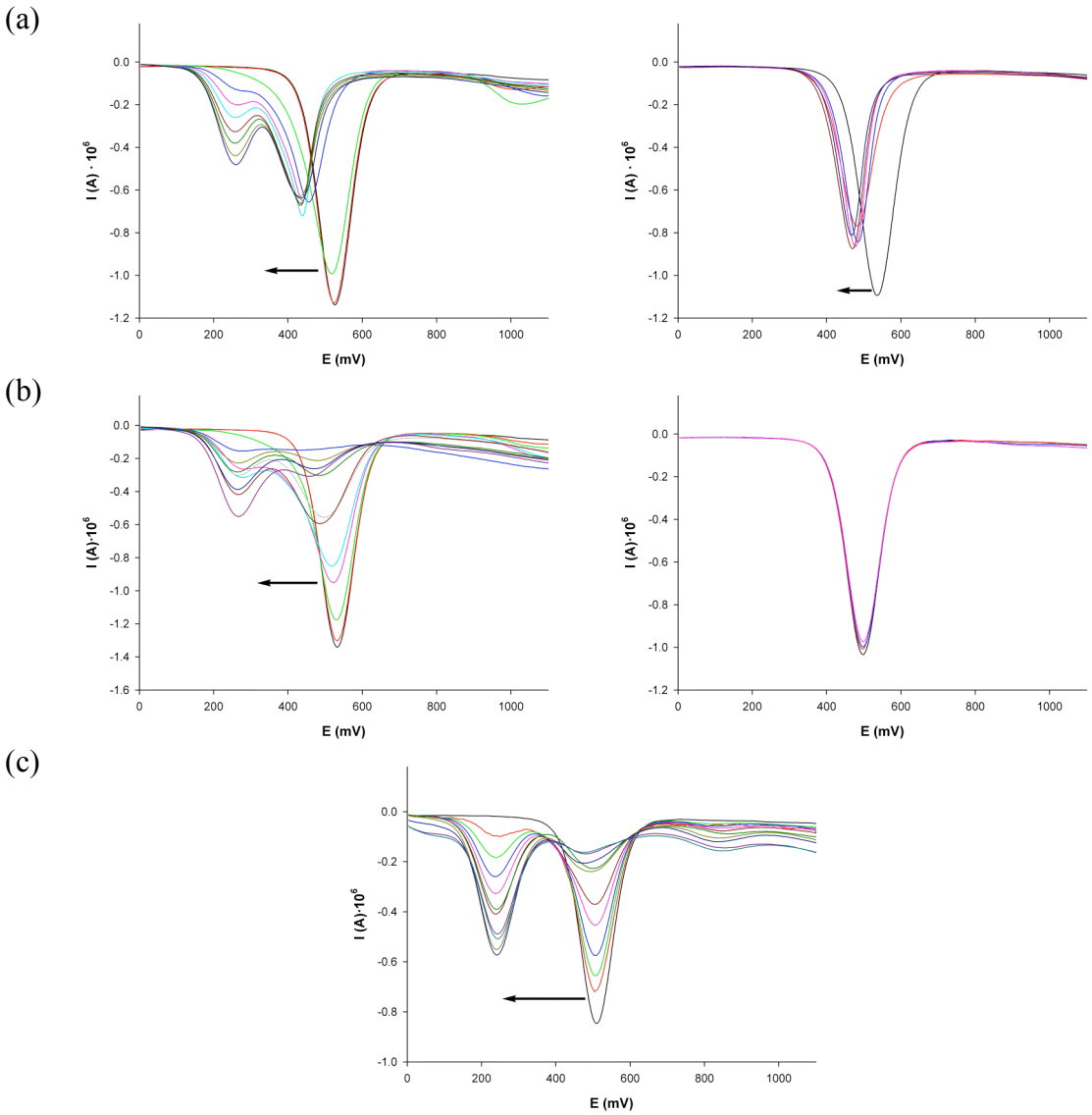

Figure SI 6. (a) Evolution of the OSWV of **6b** (1 mM) in $CH_3CN/[(n\text{-}Bu)_4]ClO_4$ scanned at 0.1 V s^{-1} in the presence of increasing amounts of (a) $HP_2O_7^{3-}$ (left) until 2 equiv and in the presence of 2 equiv of $HP_2O_7^{-3}$ and 20 equiv of acetic acid in CH_3CN (right); (b) F^- (left) until 2 equiv and in the presence of 2 equiv of F^- and 20 equiv of acetic acid in CH_3CN (right). (c) Evolution of the OSWV of **6b** (1 mM) in $CH_3CN/[(n\text{-}Bu)_4]ClO_4$ scanned at 0.1 V s^{-1} in the presence of increasing amounts of OH^- until 2 equiv.

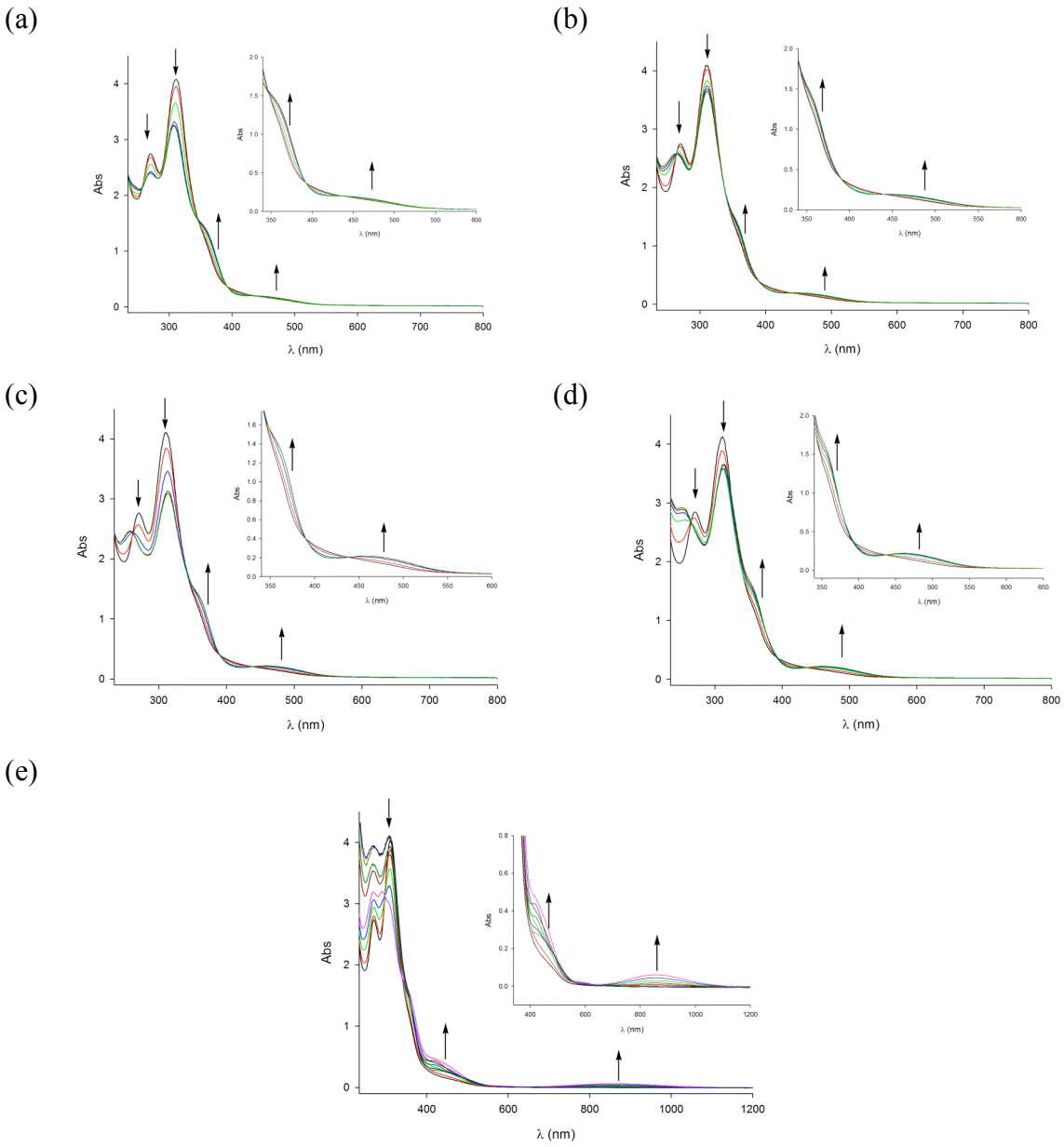

Figure SI 7. Changes in the absorption spectra of **6a** (c = $1 \cdot 10^{-4}$ M in CH_3CN) upon addition of increasing amounts of (a) Cd^{2+}; (b) Zn^{2+}; (c) Hg^{2+}; (d) Pb^{2+}; (e) Cu^{2+} metal cation, until 1 equiv was added. Arrows indicate absorptions that increase or decrease during the experiment.

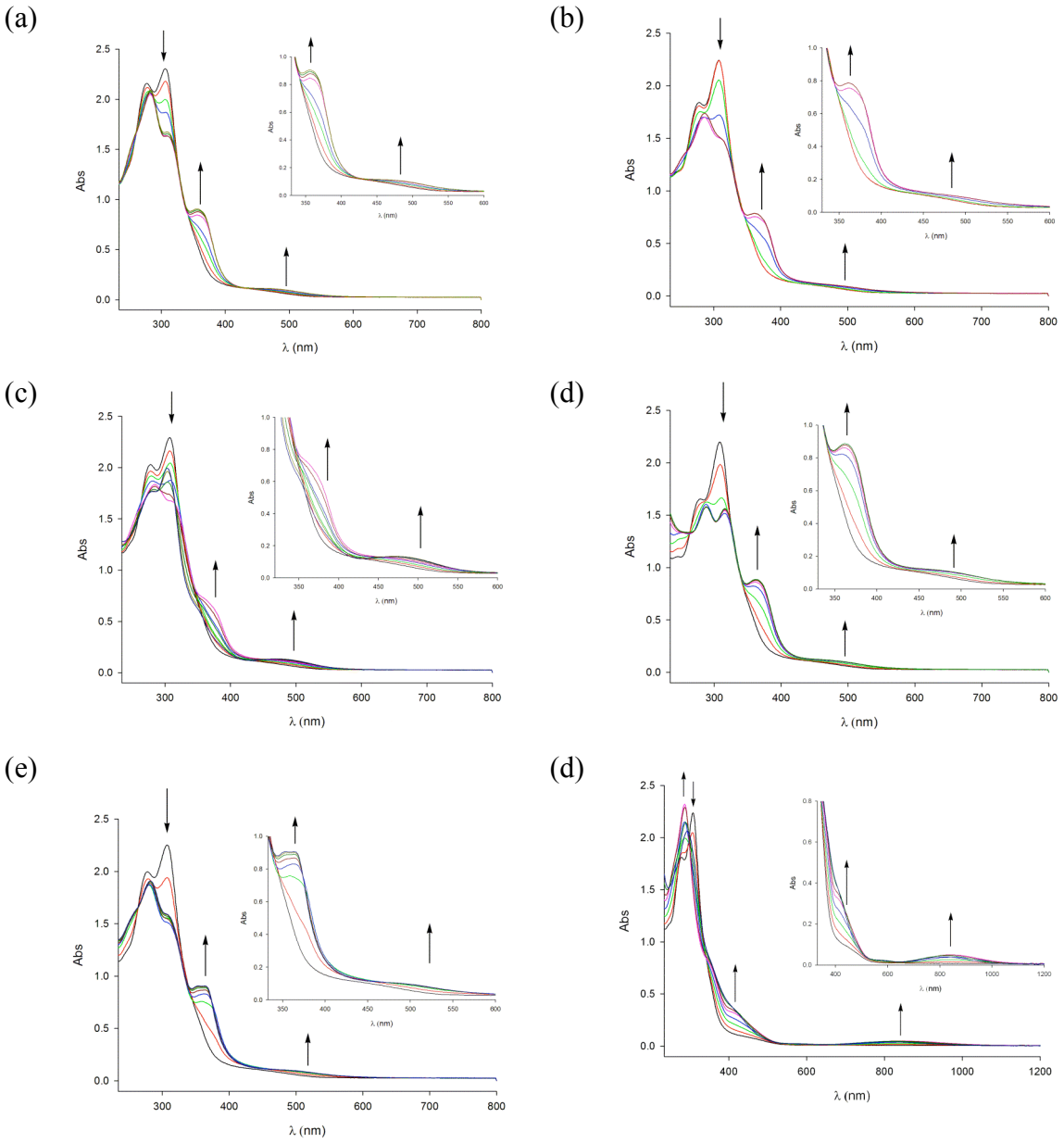

Figure SI 8. Changes in the absorption spectra of **6b** (c = $5 \cdot 10^{-5}$ M in CH_3CN) upon addition of increasing amounts of (a) Cd^{2+}; (b) Zn^{2+}; (c) Hg^{2+}; (d) Pb^{2+}; (e) Ni^{2+};(d) Cu^{2+} metal cation, until 1 equiv was added. Arrows indicate absorptions that increase or decrease during the experiment.

(a)

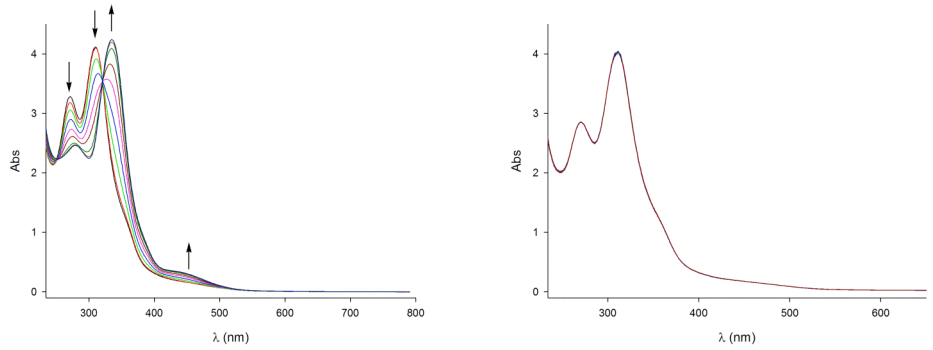

(b)

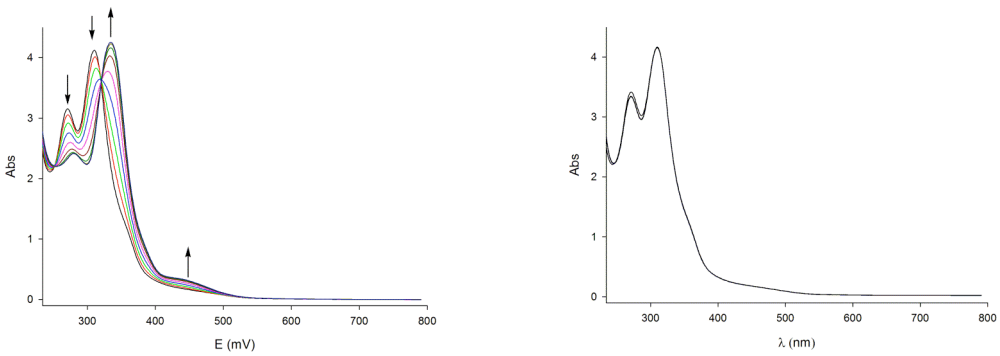

(c)

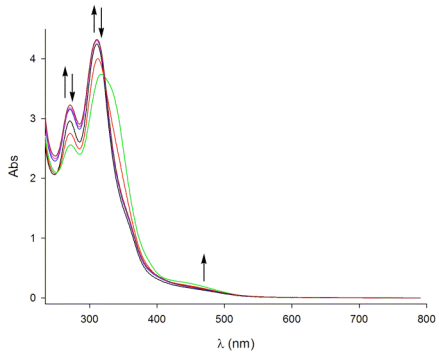

Figure SI 9. Changes in the absorption spectra of **6a** (c = $1 \cdot 10^{-4}$M in CH_3CN) upon addition of increasing amounts of (a) $HP_2O_7^{-3}$ anion; (b) F^- anion, until 2 equiv (left) and in the present of 20 equiv of acetic acid (right). (c) Changes in the absorption spectra of **6a** (c = $1 \cdot 10^{-4}$M in CH_3CN) upon addition of increasing amounts of (a) OH^- anion. Arrows indicate absorptions that increase or decrease during the experiment.

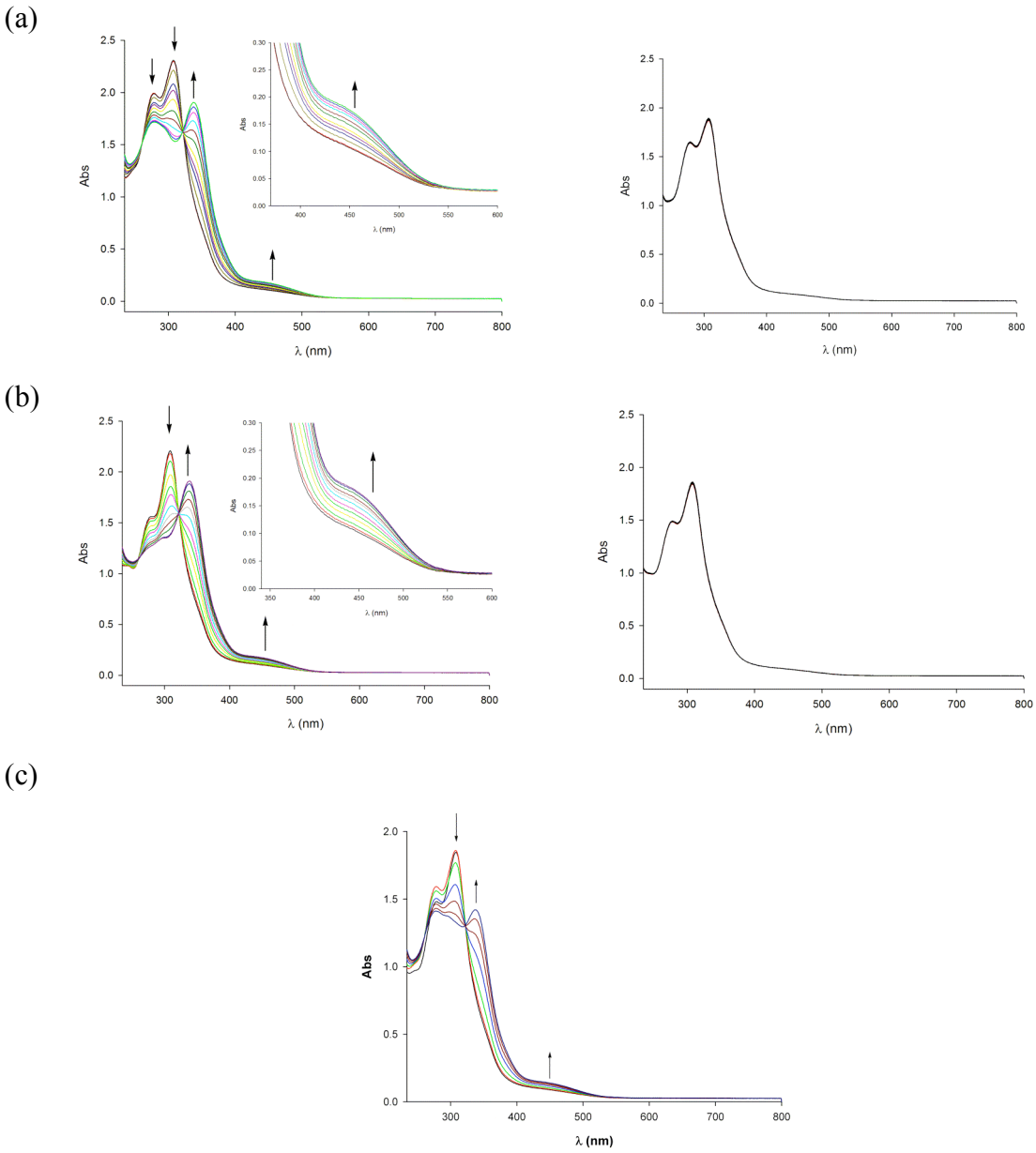

Figure SI 10. Changes in the absorption spectra of **6b** (c = $1 \cdot 10^{-4}$M in CH_3CN) upon addition of increasing amounts of (a) $HP_2O_7^{-3}$ anion; (b) F^- anion, until 2 equiv (left) and in the present of 20 equiv of acetic acid (right). (c) Changes in the absorption spectra of **6b** (c = $1 \cdot 10^{-4}$M in CH_3CN) upon addition of increasing amounts of (a) OH^- anion. Arrows indicate absorptions that increase or decrease during the experiment.

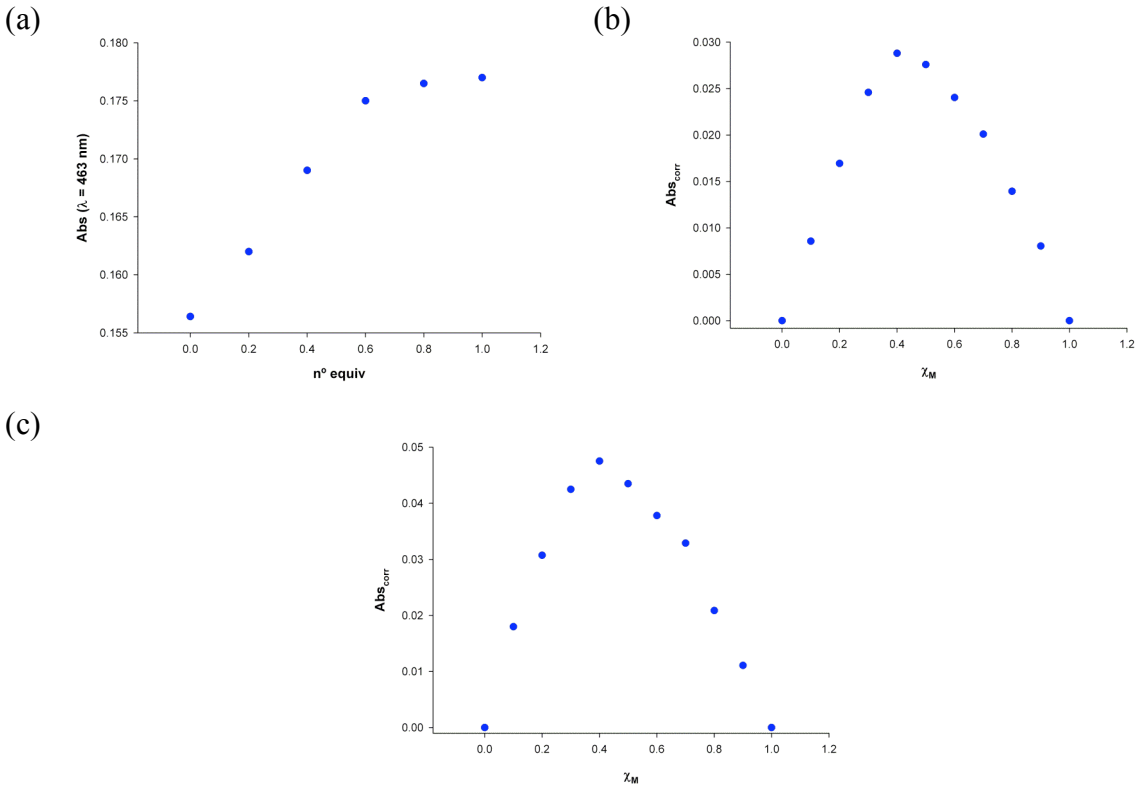

Figure SI 11. (a) Titration profile showing the change in absorbance of **6a** (c = $1 \cdot 10^{-4}$M in CH_3CN), at λ = 463 nm, upon addition of Cd^{2+}, indicating the formation of 2:1 complex. (b) Job's plot for **6a** ($1x10^{-4}$ M in CH_3CN) and Zn^{2+}, indicating the formation of a 2:1 complex. (c) Job's plot for **6a** ($1x10^{-4}$ M in CH_3CN) and Hg^{2+} ($1x10^{-4}$ M in CH_3CN), indicating the formation of a 2:1 complex.

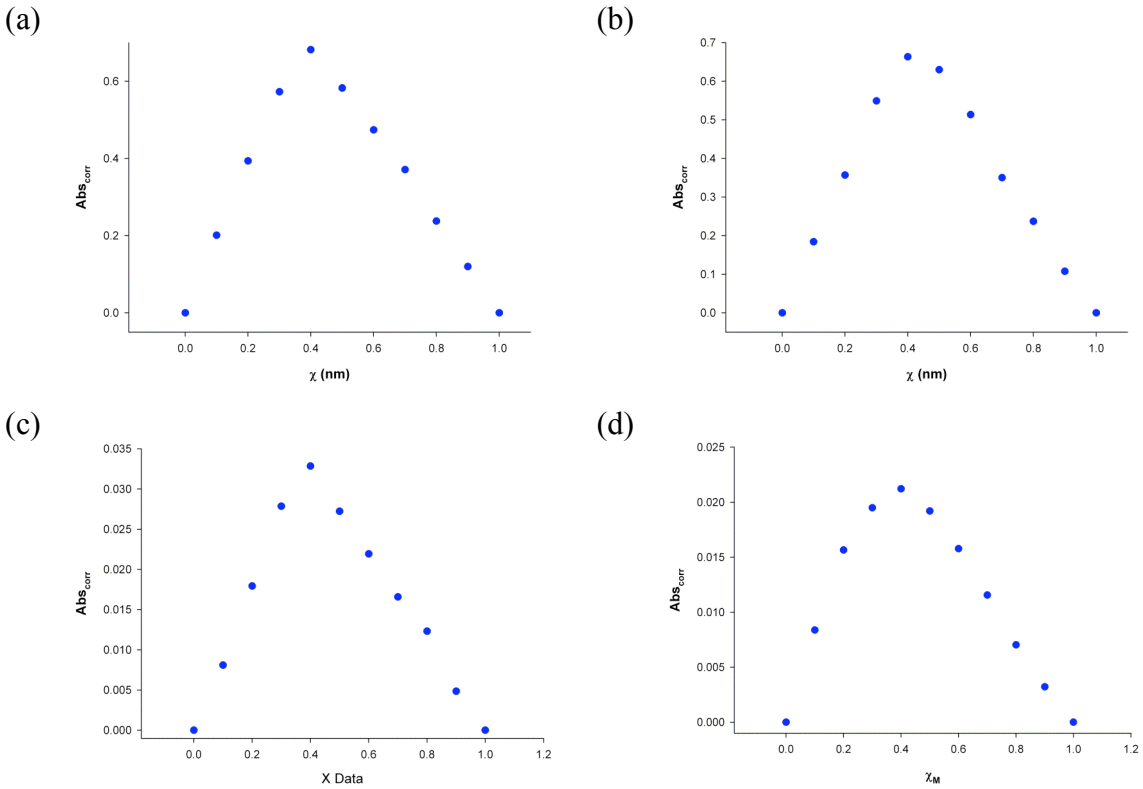

Figure SI 12. Job's plot for **6b** ($1x10^{-4}$ M in CH_3CN), and (a) Cd^{2+}; (b) Zn^{2+}; (c) Pb^{2+}; (d) Ni^{2+} ($1x10^{-5}$ M in CH_3CN), indicating the formation of 2:1 complexes.

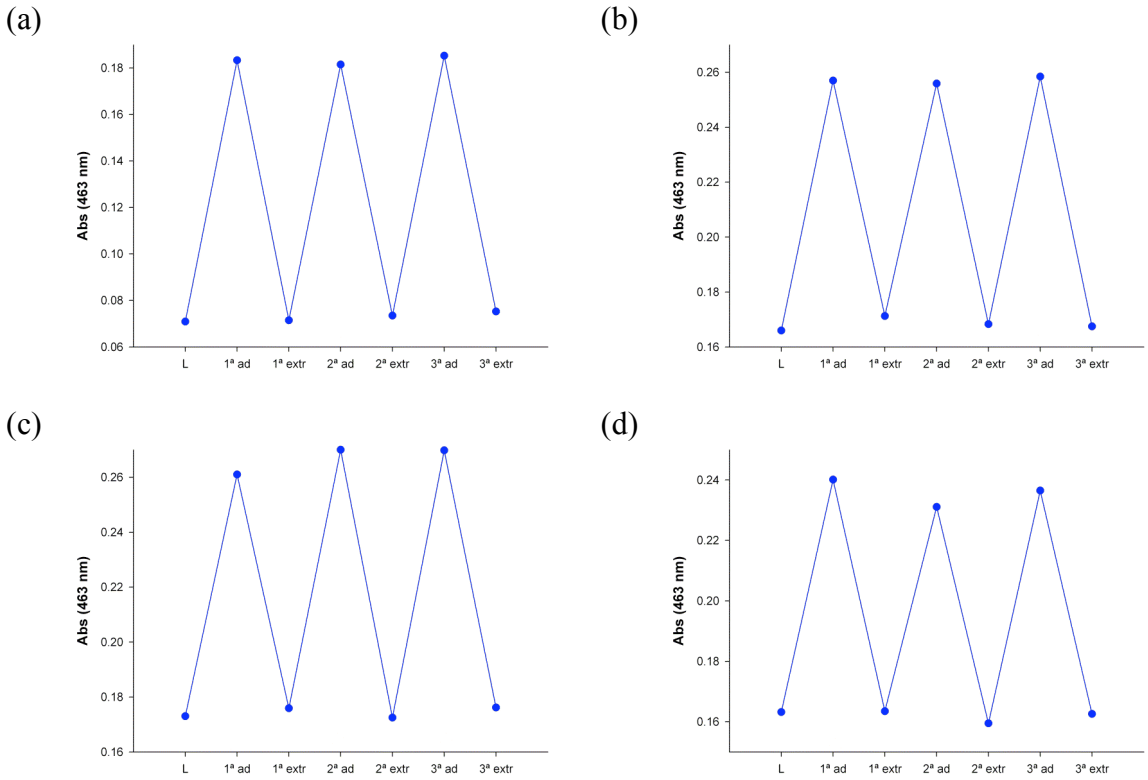

Figure SI 13. Stepwise complexation [by addition of (a) Cd^{2+}; (b) Zn^{2+}; (c) Hg^{2+}; (d) Pb^{2+}]/decomplexation (extraction with H_2O) cycles of ligand **6a** (c = $1x10^{-4}$M in CH_2Cl_2) carried out by UV/Vis analysis.

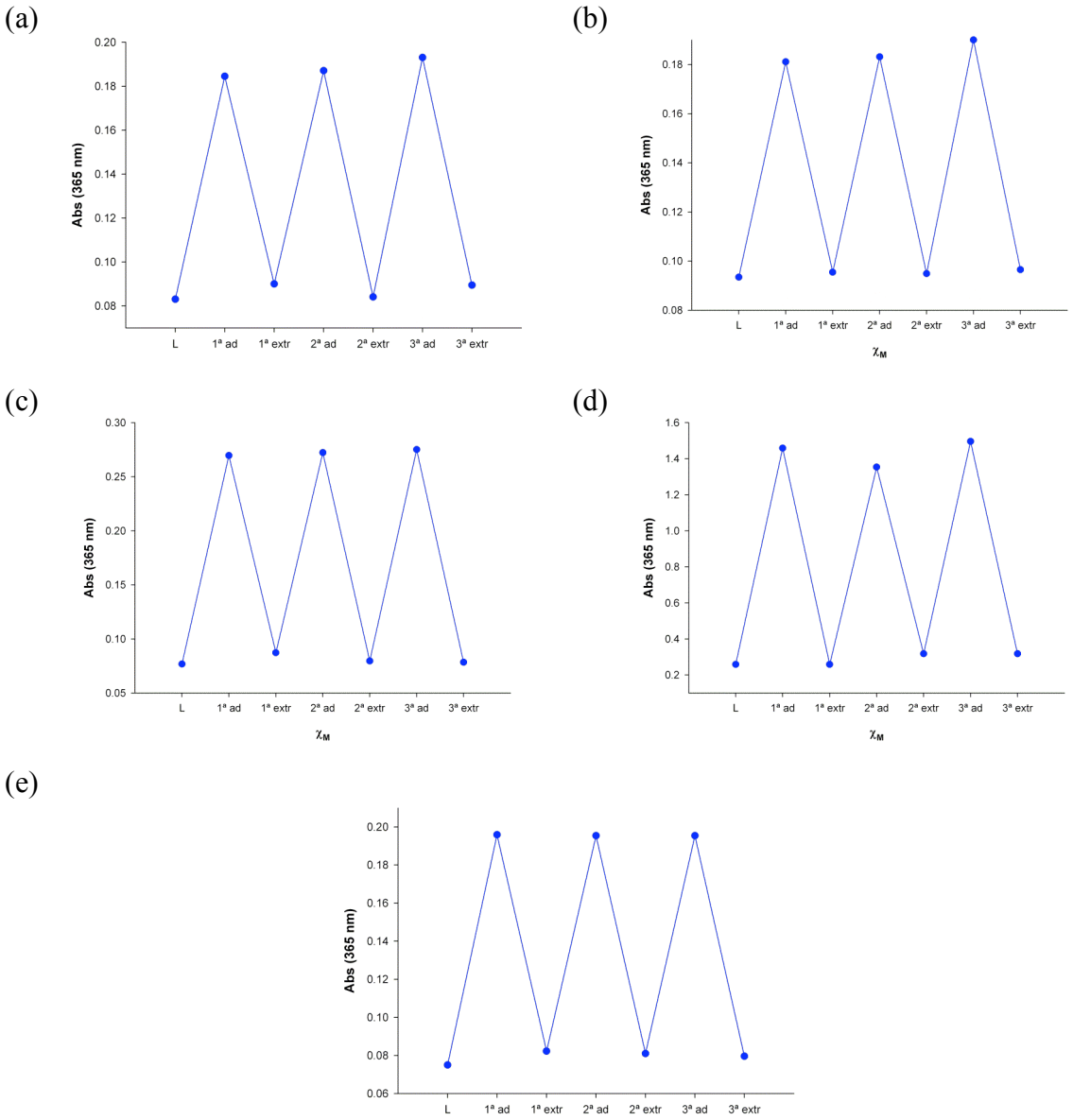

Figure SI 14. Stepwise complexation [addition of (a) Cd^{2+}; (b) Zn^{2+}; (c) Hg^{2+}; (d) Pb^{2+}; (e) Ni^{2+}]/decomplexation (extraction with H_2O) cycles of ligand **6b** (c = $1x10^{-4}$M in CH_2Cl_2) carried out by UV/Vis analysis.

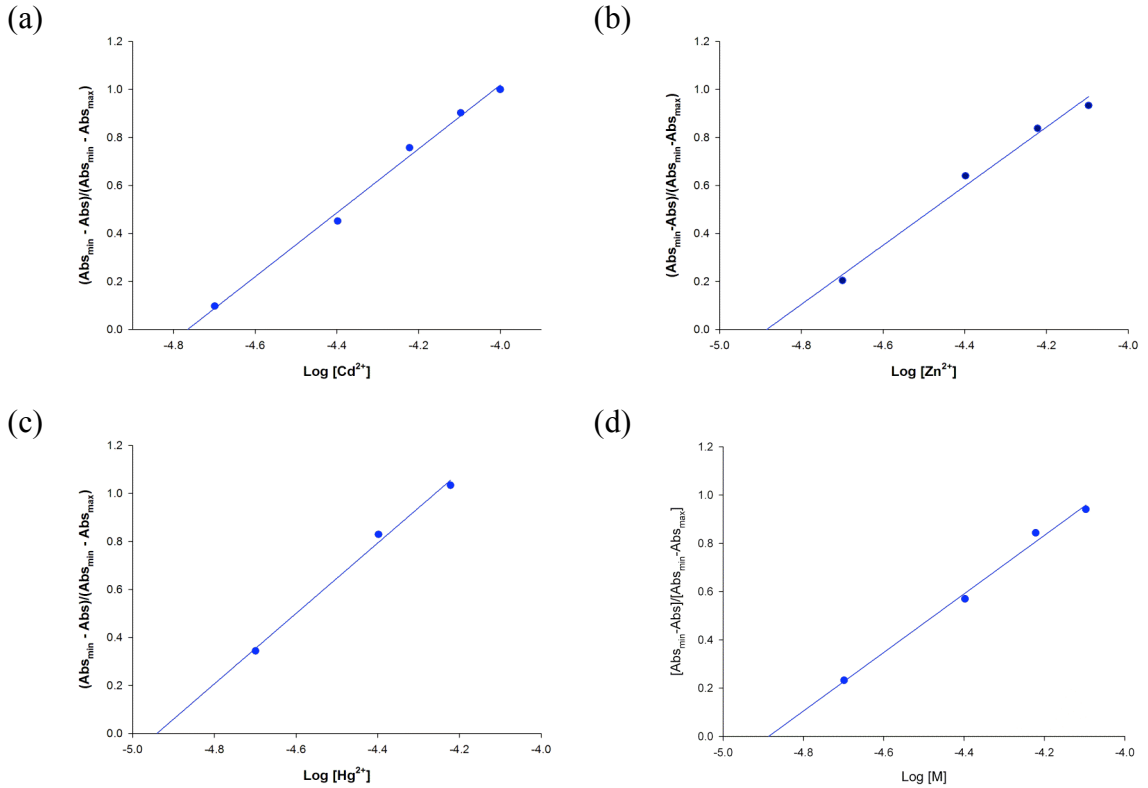

Figure SI 15. Absorbance of **6a** (c = $1 \cdot 10^{-4}$M in CH_3CN) at each concentration of cation added (a) Cd^{2+}; (b) Zn^{2+}; (c) Hg^{2+}; (d) Pb^{2+}, normalized between the minimum absorbance, found at zero equiv of metal cation; and the maximum absorbance, found at (a) $[Cd^{2+}]=1.72 \cdot 10^{-5}$ M; (b) $[Zn^{2+}]=1.31 \cdot 10^{-5}$ M; (c) $[Hg^{2+}]=1.15 \cdot 10^{-5}$ M; (d) $[Pb^{2+}]=1.30 \cdot 10^{-5}$ M.

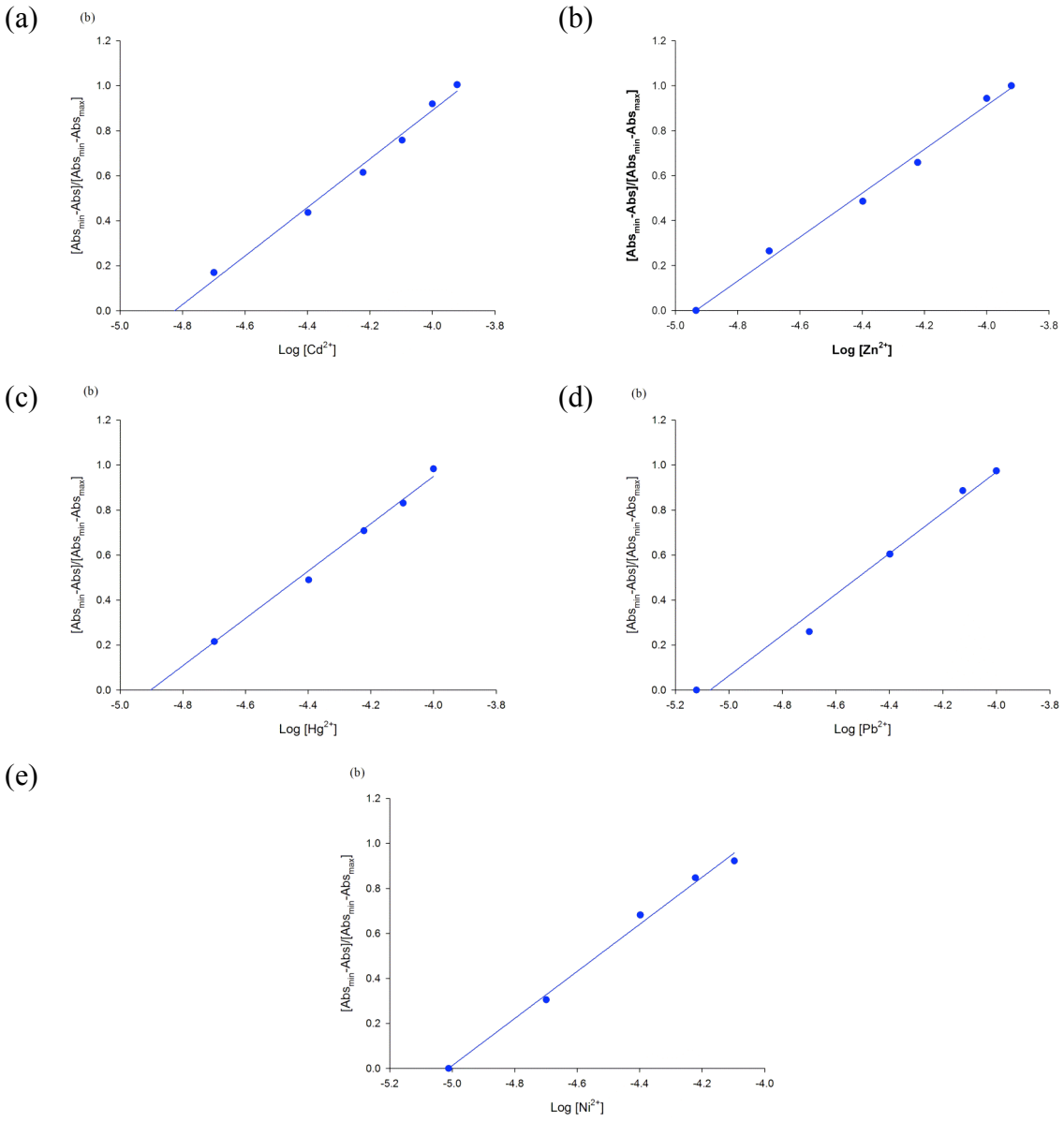

Figure SI 16. Absorbance of **6b** (c = $1 \cdot 10^{-4}$M in CH_3CN) at each concentration of cation added (a) Cd^{2+}; (b) Zn^{2+}; (c) Hg^{2+}; (d) Pb^{2+}; (e) Ni^{2+} normalized between the minimum absorbance, found at zero equiv of metal cation; and the maximum absorbance, found at (a) $[Cd^{2+}]=1.50 \cdot 10^{-5}$ M; (b) $[Zn^{2+}]=1.16 \cdot 10^{-5}$ M; (c) $[Hg^{2+}]=1.25 \cdot 10^{-5}$ M; (d) $[Pb^{2+}]=7.58 \cdot 10^{-6}$ M; (e) $[Ni^{2+}]=9.74 \cdot 10^{-6}$ M.

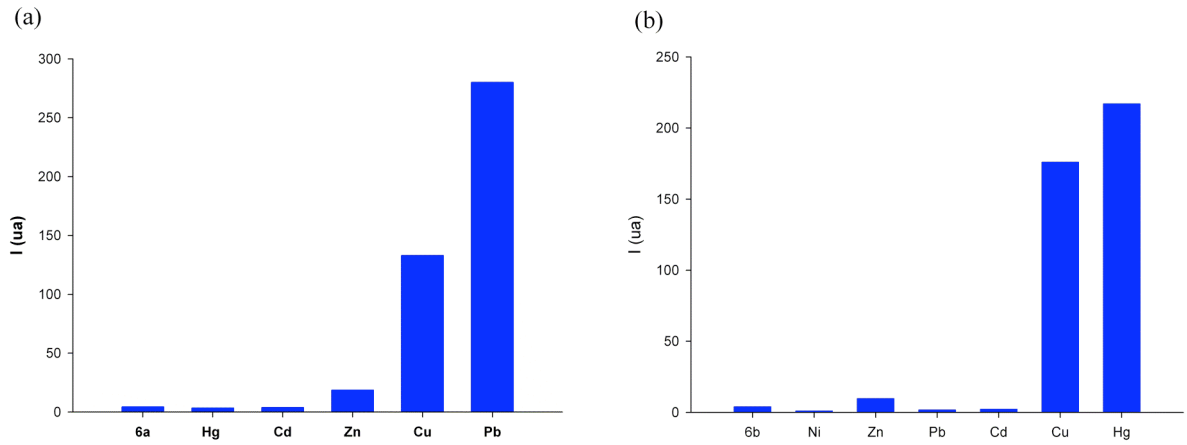

Figure SI 17. Fluorescence intensity of ligand (a) **6a**; (b) **6b**, in CH_3CN, after addition of 1 equiv of several cations. Emission monitored at (a) λ_{exc} = 330 nm; (b) λ_{exc} = 310 nm.

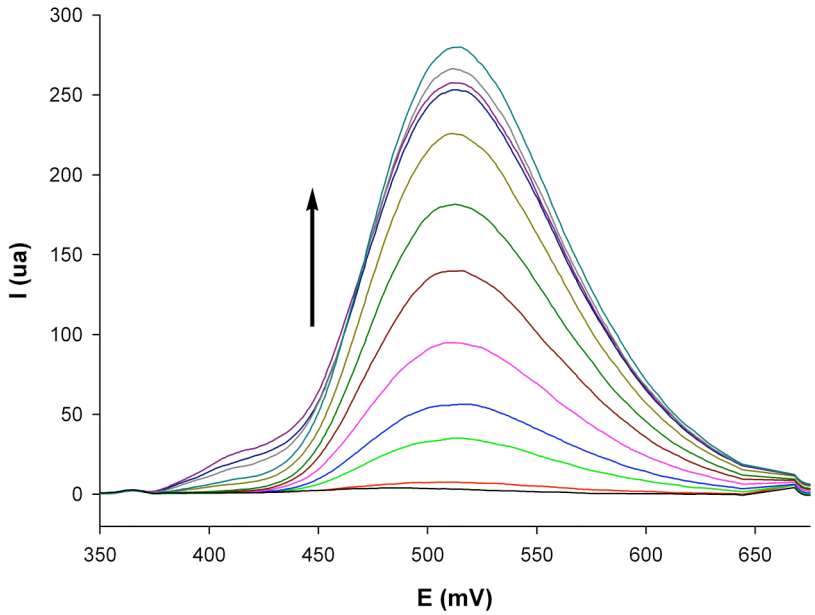

Figure SI 18. Changes in the fluorescence emission spectrum of **6a** (c = 1 x 10^{-5} M in CH_3CN) upon titration with Pb^{2+}: the initial (black) is that of **6a** and the final one (deep cyan), after addition of 1.4 equiv of Pb^{2+} (c = 2.5x10^{-3} M in CH_3CN). Emission is monitored at λ_{exc} = 330 nm.

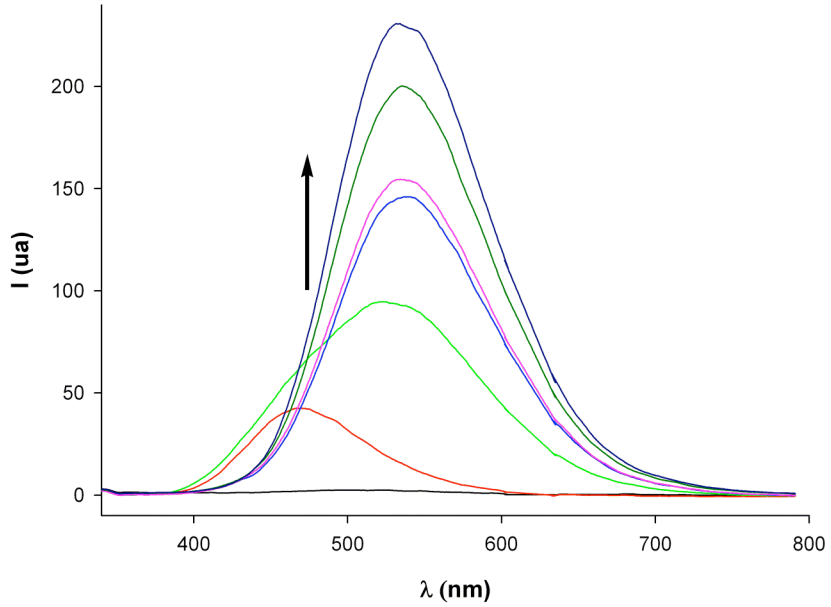

Figure SI 19. Changes in the fluorescence emission spectrum of **6b** (c = 1 x 10^{-5} M in CH_3CN) upon titration with Hg^{2+}: the initial (black) is that of **6b** and the final one (deep blue), after addition of 1.2 equiv of Hg^{2+} (c = 2.5x10^{-3} M in CH_3CN). Emission is monitored at λ_{exc} = 310 nm.

(a) (b)

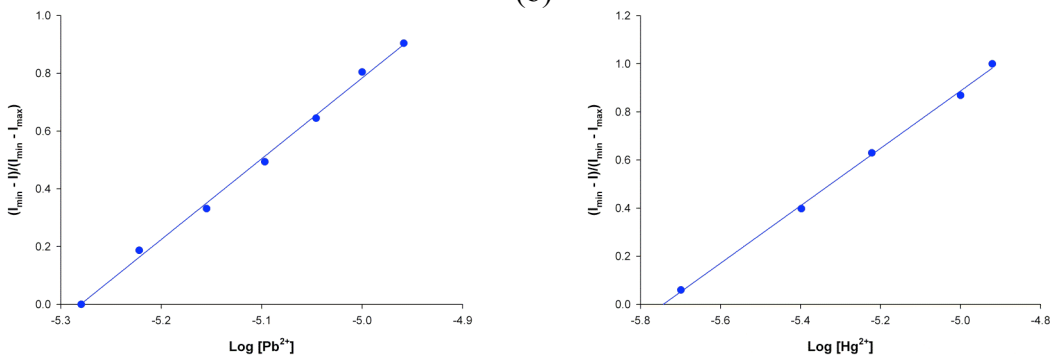

Figure SI 20. Fluorescence intensity of (a) **6a**; (b) **6b** (1x10^{-5} M in CH_3CN), at each concentration of (a) Pb^{2+}; (b) Hg^{2+} added, normalized between the minimum fluorescence intensity, found at zero equiv of cation, and the maximum fluorescence intensity, found at (a) [Pb^{2+}]= 5.25x10^{-6} M; (b) [Hg^{2+}]= 1.81x10^{-6} M.

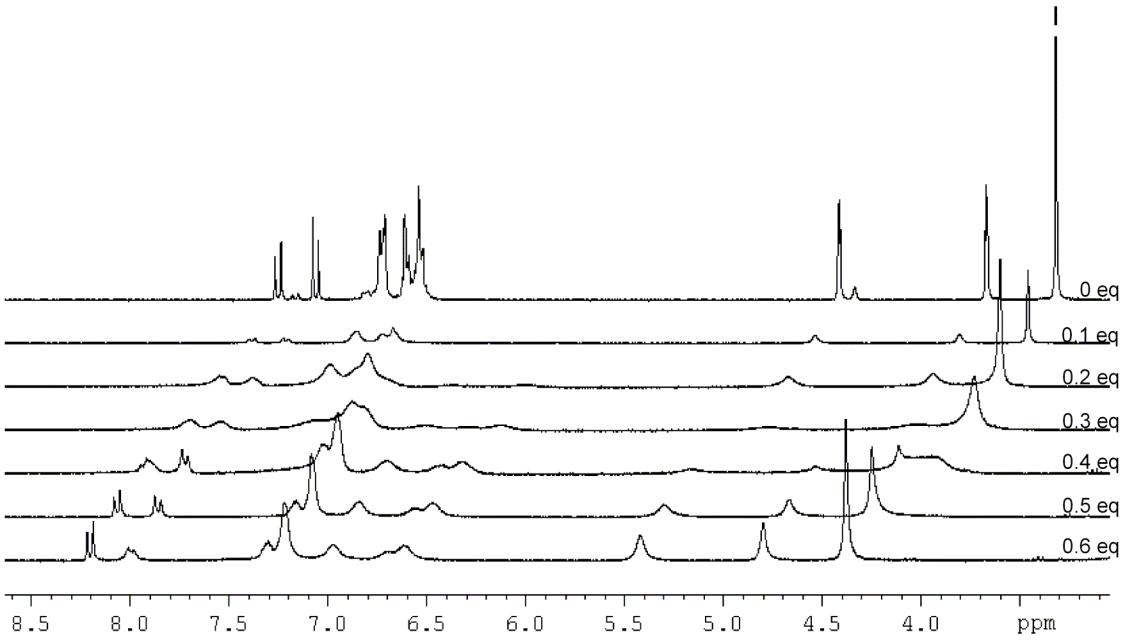

Figure SI 21. Changes in the ^{1}H-NMR (in acetone-d_6) spectrum of **6a** (top) in acetone upon addition of increasing amounts of Cd^{2+} until 0.6 equiv (bottom).

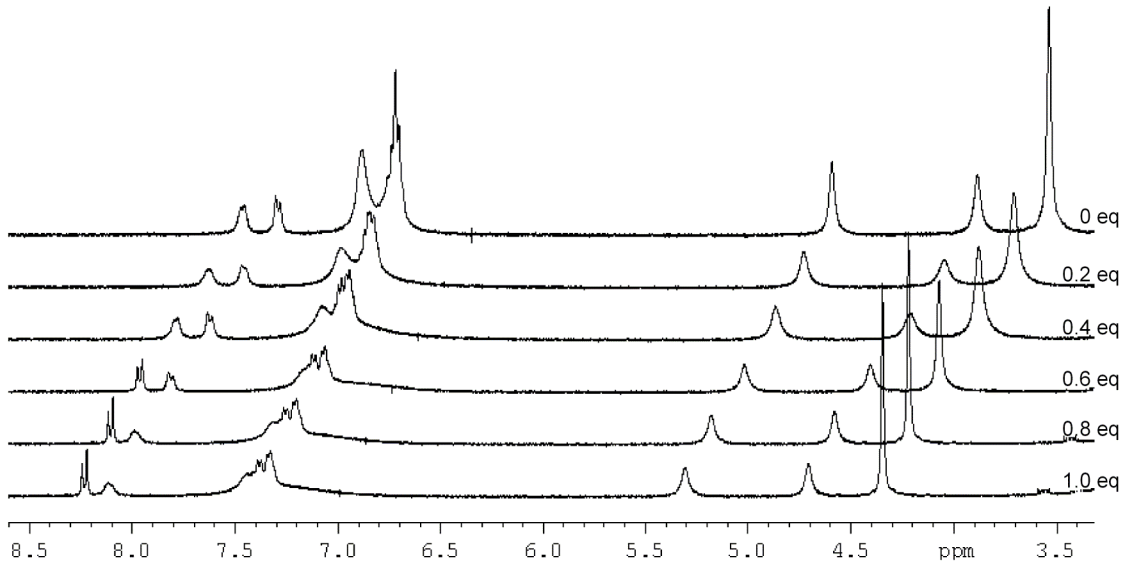

Figure SI 22. Changes in the ^{1}H-NMR (in acetone-d_6) spectrum of **6a** (top) in acetone upon addition of increasing amounts of Zn^{2+} until 1.0 equiv (bottom).

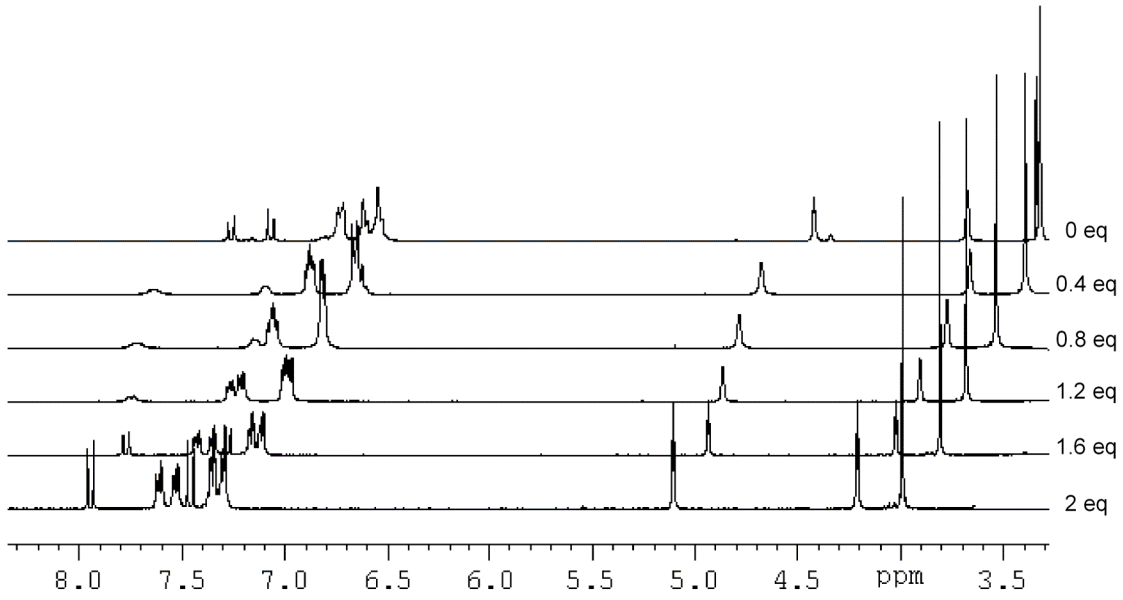

Figure SI 23. Changes in the ^{1}H-NMR (in acetone-d_6) spectrum of **6a** (top) in acetone upon addition of increasing amounts of $HP_2O_7^{3-}$ until 2.0 equiv (bottom).

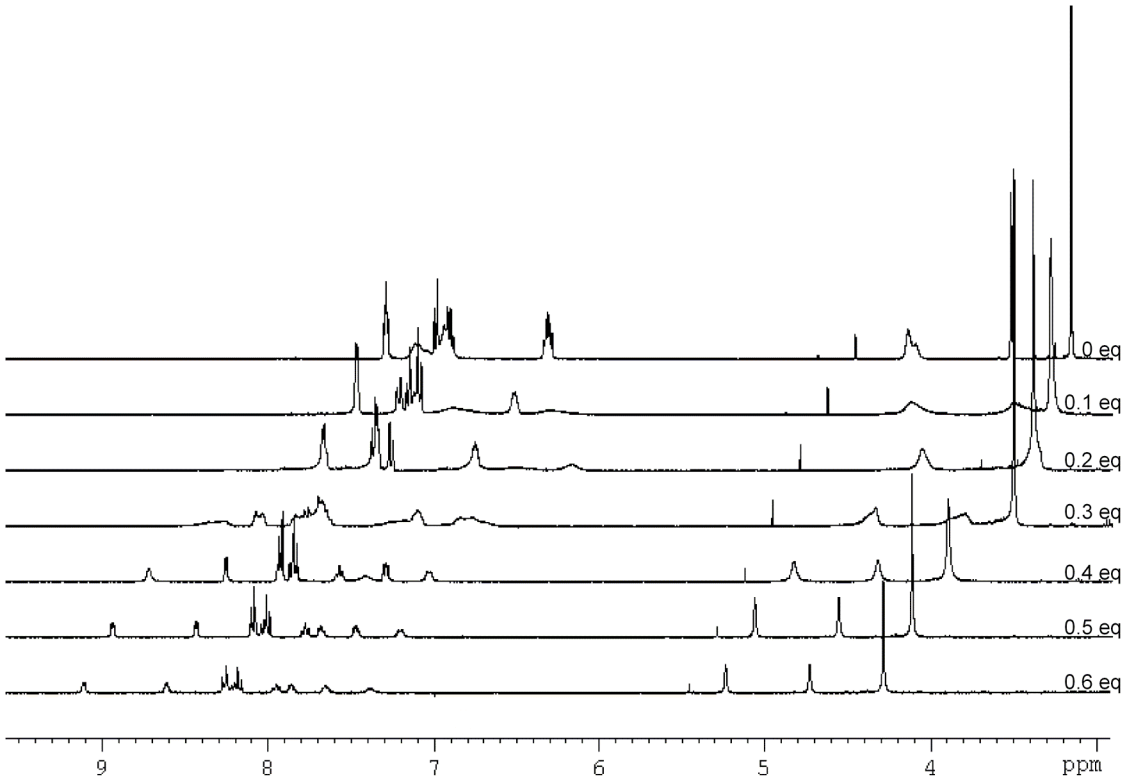

Figure SI 24. Changes in the ^{1}H-NMR (in acetonitrile-d_3) spectrum of **6b** (top) in acetone upon addition of increasing amounts of Pb^{2+} until 0.6 equiv (bottom).

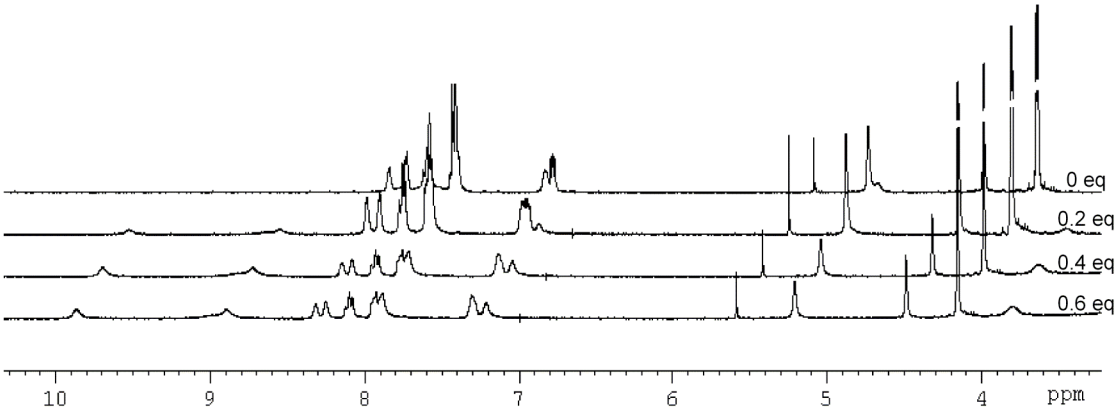

Figure SI 25. Changes in the ^{1}H-NMR (in acetone-d_6) spectrum of **6b** (top) in acetone upon addition of increasing amounts of Ni^{2+} until 0.6 equiv (bottom).

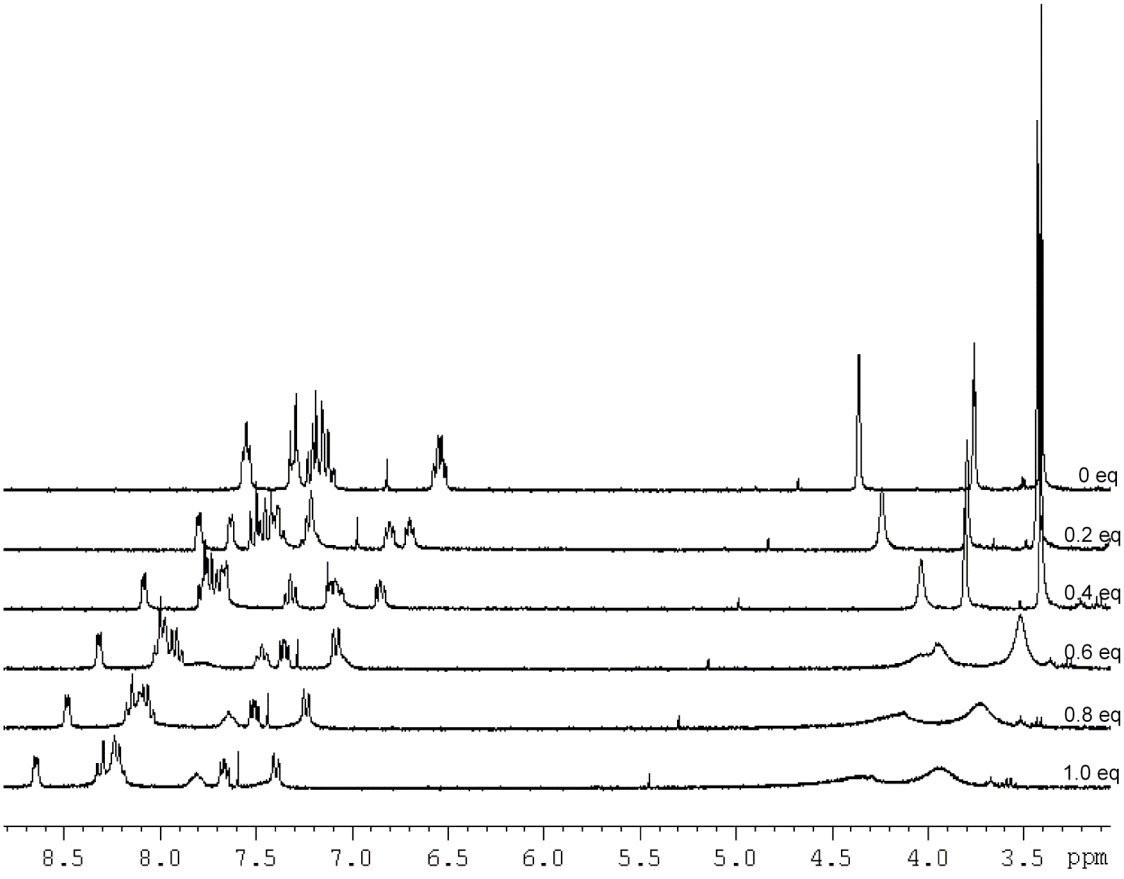

Figure SI 26. Changes in the ^{1}H-NMR (in acetonitrile-d_3) spectrum of **6b** (top) in acetone upon addition of increasing amounts of Cd^{2+} until 1.0 equiv (bottom).

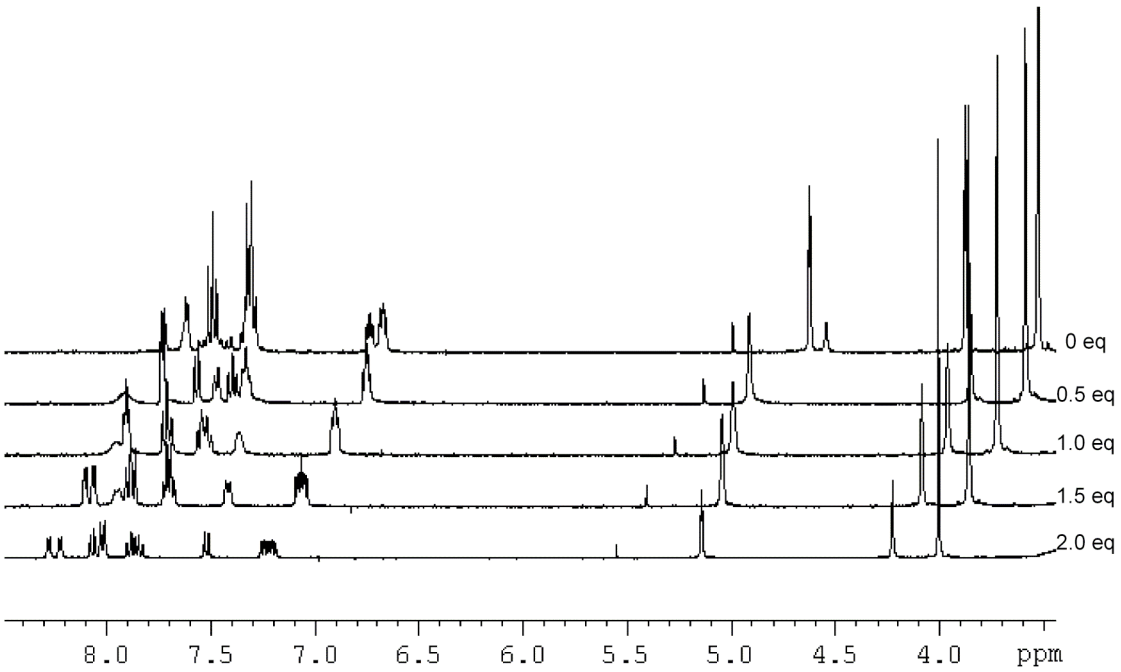

Figure SI 27. Changes in the ^{1}H-NMR (in acetone-d_6) spectrum of **6b** (top) in acetone upon addition of increasing amounts of $HP_2O_7^{3-}$ until 2.0 equiv (bottom).

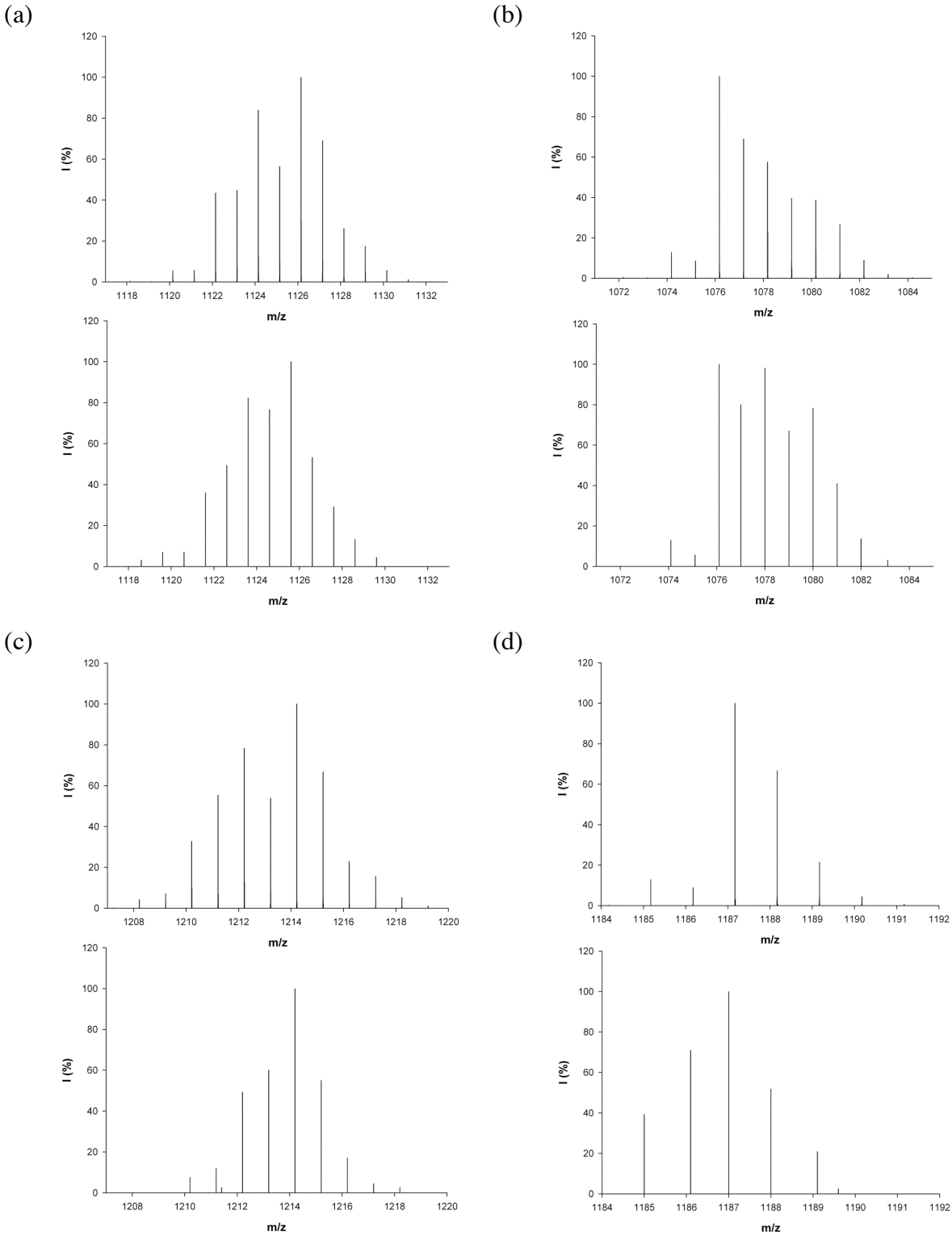

Figure SI 28. Relative abundance of the isotopic cluster for (a) $\mathbf{6a_2 \cdot Cd^{2+}}$; (b) $\mathbf{6a_2 \cdot Zn^{2+}}$; (c) $\mathbf{6a_2 \cdot Hg^{2+}}$; (d) $\mathbf{6a_2 \cdot HP_2O_7^{3-}}$ (top) simulated; (bottom) experimental.

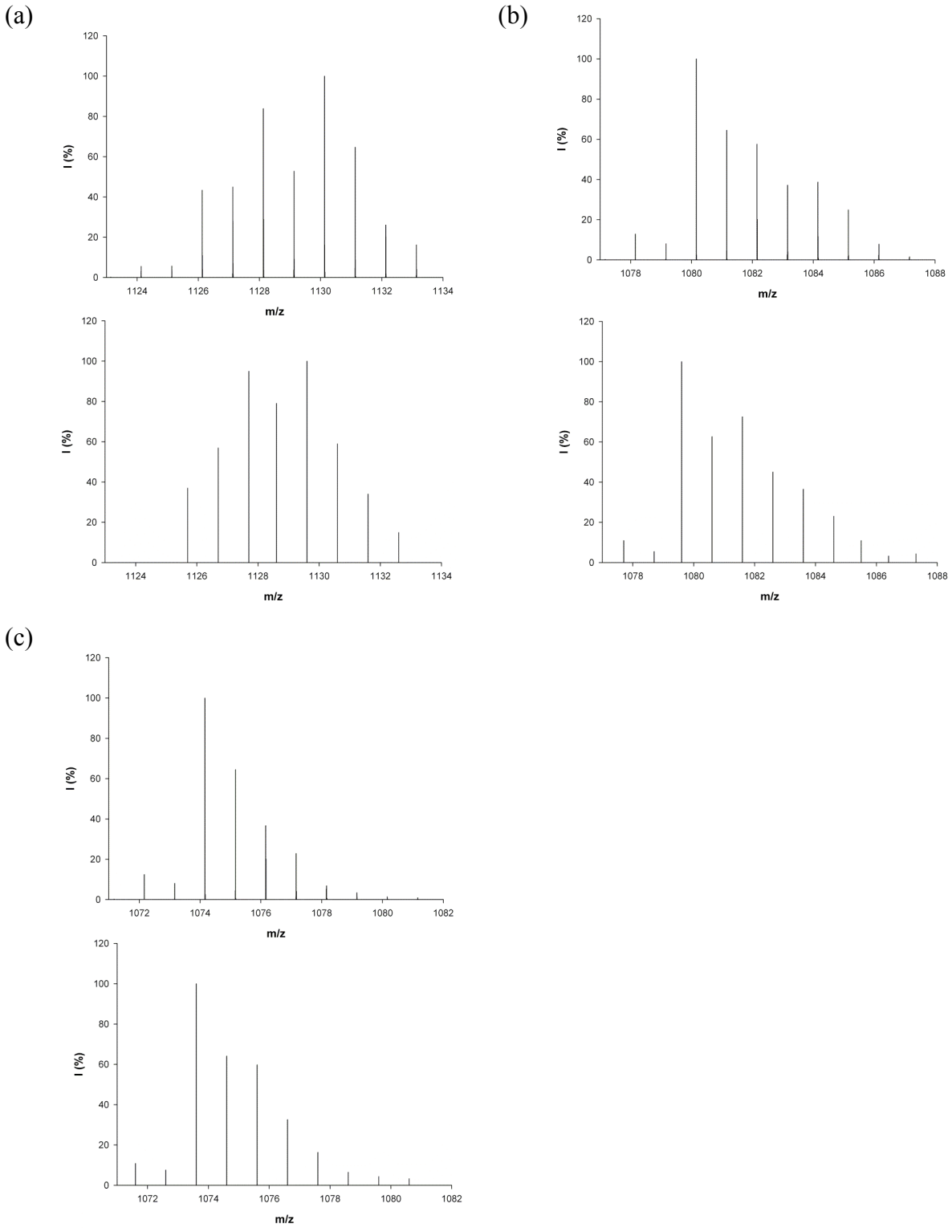

Figure SI 29. Relative abundance of the isotopic cluster for (a) $\mathbf{6b_2{\cdot}Cd^{2+}}$; (b) $\mathbf{6b_2{\cdot}Zn^{2+}}$; (c) $\mathbf{6c_2{\cdot}Ni^{2+}}$ (top) simulated; (bottom) experimental.